The chemotherapeutic drug doxorubicin does not exacerbate p16^{Ink4a}-positive senescent cell accumulation and cardiometabolic disease development in young adult female LDLR-deficient mice

Postmus, Andrea C.; Kruit, Janine K.; Eilers, Roos E.; Havinga, Rick; Koster, Mirjam H.; Johmura, Yoshikazu; Nakanishi, Makoto; van de Sluis, Bart; Jonker, Johan W.

Published in:
Toxicology and Applied Pharmacology

DOI:
10.1016/j.taap.2023.116531

Publication date:
2023

Toxicology and Applied Pharmacology 468 (2023) 116531

Contents lists available at ScienceDirect

Toxicology and Applied Pharmacology

journal homepage: www.elsevier.com/locate/taap

The chemotherapeutic drug doxorubicin does not exacerbate p16^{Ink4a}-positive senescent cell accumulation and cardiometabolic disease development in young adult female LDLR-deficient mice

Andrea C. Postmus [a], Janine K. Kruit [a], Roos E. Eilers [a], Rick Havinga [a], Mirjam H. Koster [a], Yoshikazu Johmura [b], Makoto Nakanishi [c], Bart van de Sluis [a], Johan W. Jonker [a,*]

[a] Department of Pediatrics, University of Groningen, University Medical Center Groningen, Groningen, The Netherlands
[b] Division of Cancer and Senescence Biology, Cancer Research Institute, Institute for Frontier Science Initiative, Kanazawa University, Kakuma, Kanazawa, Japan
[c] Division of Cancer Cell Biology, Institute of Medical Science, University of Tokyo, Tokyo, Japan

ARTICLE INFO

Editor: Lawrence Lash

Keywords:
Cancer survivor
Chemotherapy
Doxorubicin
Cellular senescence
Cardiometabolic disease

ABSTRACT

Cancer survivors who received chemotherapy, such as the anthracycline doxorubicin (DOX), have an increased risk of developing complications later in life, including the development of chronic metabolic diseases. Although the etiology of this increased risk for late metabolic complications in cancer survivors is poorly understood, a causal role of therapy-induced senescent cells has been suggested.

To study the role of cellular senescence in chemotherapy-induced metabolic complications, young adult female low-density lipoprotein receptor-deficient *(Ldlr$^{-/-}$)-p16-3MR* mice, in which p16^{Ink4a}-positive (p16^{Ink4a+}) senescent cells can be genetically eliminated, were treated with four weekly injections of DOX (2.5 mg/kg) followed by a high-fat high-cholesterol diet for 12 weeks. While DOX treatment induced known short-term effects, such as reduction in body weight, gonadal fat mass, and adipose tissue inflammation, it was not associated with significant long-term effects on glucose homeostasis, hepatic steatosis, or atherosclerosis. We further found no evidence of DOX-induced accumulation of p16^{Ink4a+}-senescent cells at 1 or 12 weeks after DOX treatment. Neither did we observe an effect of elimination of p16^{Ink4a+}-senescent cells on the development of diet-induced cardiometabolic complications in DOX-treated mice. Other markers for senescence were generally also not affected except for an increase in *p21* and *Cxcl10* in gonadal white adipose tissue long-term after DOX treatment.

Together, our study does not support a significant role for p16^{Ink4a+}-senescent cells in the development of diet-induced cardiometabolic disease in young adult DOX-treated female *Ldlr$^{-/-}$* mice. These findings illustrate the need of further studies to understand the link between cancer therapy and cardiometabolic disease development in cancer survivors.

1. Introduction

Survival rates of cancer patients have significantly increased over the last decades due to advancements in therapy (Bleyer et al., 2006; Keegan et al., 2016; Liu et al., 2019). As a consequence, long-term adverse effects of cancer therapy are rapidly becoming a major cause of morbidity and mortality (Dowling et al., 2013). Pediatric and adult-onset cancer survivors show accelerated ageing and are at increased risk of developing chronic cardiometabolic disease, such as type 2 diabetes, non-alcoholic fatty liver disease (NAFLD), and atherosclerosis, which present years after completion of their treatment (Ben-Yakov et al., 2018; de Haas et al., 2010; Juanjuan et al., 2015; Smitherman et al., 2020; Stelwagen et al., 2020).

The anthracycline doxorubicin (DOX) is one of the most effective

Abbreviations: DOX, doxorubicin; LDLR, low-density lipoprotein receptor; NAFLD, non-alcoholic fatty liver disease; ROS, reactive oxygen species; SASP, senescence-associated secretory phenotype; mRFP, monomeric red fluorescent protein; HSV-TK, herpes simplex virus thymidine kinase; GCV, ganciclovir; i.p., intraperitoneal; HFC, high-fat high-cholesterol; TAM, tamoxifen; TOM, tdTomato; LV, left-ventricular; oGTT, oral glucose tolerance test; ITT, insulin tolerance test; ALT, alanine aminotransferase; AST, aspartate aminotransferase; H&E, hematoxylin-eosin; CLS, crown-like structure; gWAT, gonadal white adipose tissue; mWAT, mesenteric white adipose tissue; scWAT, subcutaneous white adipose tissue; WBC, white blood cell; ANP, atrial natriuretic peptide.

* Corresponding author.
E-mail address: j.w.jonker@umcg.nl (J.W. Jonker).

https://doi.org/10.1016/j.taap.2023.116531
Received 8 March 2023; Received in revised form 5 April 2023; Accepted 19 April 2023
Available online 23 April 2023

anti-cancer drugs and widely used to treat a variety of cancers including hematological and solid malignancies (Young et al., 1981). However, the clinical use of DOX is restricted due to its severe toxic effects on multiple tissues such as the heart, liver, kidney, adipose, vasculature, and reproductive system (Mohan et al., 2021; Prasanna et al., 2020; Rahimi et al., 2022; Lahoti et al., 2012; Vergoni et al., 2016; Volkova and Russell, 2011). Cancer patients usually receive multiple chemotherapeutic drugs combined with radiotherapy or surgery making it difficult to study potential long-term cardiometabolic effects induced by DOX in clinical studies. However, studies in animal models indicate that DOX can negatively impact metabolic health. *In vivo* administration of low-dose DOX in mice resulted in adipose tissue inflammation and adipocyte insulin resistance (Vergoni et al., 2016; Biondo et al., 2018), whereas administration of high-dose DOX led to impaired systemic insulin sensitivity (de Lima Junior et al., 2016), liver damage (Renu et al., 2019), systemic inflammation (Sauter et al., 2011), and vascular damage (Rahimi et al., 2022) in different rodent models and might thereby drive the development of cardiometabolic disease such as diabetes, NAFLD, and atherosclerosis.

The primary mechanism of action of DOX is intercalation of the drug into DNA, which inhibits topoisomerase II-mediated DNA repair and results in cell cycle arrest (Thorn et al., 2011). DOX also induces the generation of reactive oxygen species (ROS) leading to oxidative stress, lipid peroxidation, and damage to DNA, cellular membranes, and proteins (Thorn et al., 2011). Unrepaired DNA damage in cells can induce apoptotic or necrotic cell death or trigger cells to go into cellular senescence, a stress response in which cells stop dividing but remain metabolically active (Childs et al., 2014; van Deursen, 2014). Senescent cells persist in tissues and can induce tissue inflammation and dysfunction through the secretion of pro-inflammatory cytokines, chemokines, and proteases, the so-called senescence-associated secretory phenotype (SASP) (Postmus et al., 2019). DOX is widely used in preclinical studies to investigate the role of cellular senescence in the pathology of diseases, including cardiometabolic disease and it has been suggested that induction of cellular senescence could be a potential mechanism by which DOX induces its long-term adverse effects (Baar et al., 2017; Baboota et al., 2022; Bonnet et al., 2022; Demaria et al., 2017; Xu et al., 2015).

So far, most rodent studies have only explored the acute effects of DOX on metabolic function up till days or weeks after a single high-dose injection. However, in clinical practice, patients receive multiple treatment cycles and cardiometabolic disease often manifests many years after completion of treatment. In the current study, we therefore investigated the long-term effects of DOX on the induction of cellular senescence and the development of cardiometabolic disease under conditions of metabolic stress in atherosclerosis-prone mice.

2. Methods

2.1. Animals

C57BL/6 J low-density lipoprotein receptor-deficient (*Ldlr*$^{-/-}$) mice (Jackson Laboratory, Bar Harbor, ME, US) were bred in house and crossed with C57BL/6 J *p16-3MR* mice, in which p16^{Ink4a}-positive (p16^{Ink4a+}) cells can be visualized (renilla luciferase, monomeric red fluorescent protein (mRFP)) and genetically eliminated (truncated herpes simplex virus 1 thymidine kinase (HSV-TK)) upon administration of ganciclovir (GCV) (Demaria et al., 2014). The *p16-3MR* mice were kindly provided by Dr. M. Demaria (European Research Institute for the Biology of Ageing, University Medical Center Groningen, The Netherlands). Experimental mice were homozygous for the *Ldlr*-knockout allele (*Ldlr*$^{-/-}$) and contained a single copy of the *3MR* transgene (*Ldlr*$^{-/-}$*-p16-3MR*). C57BL/6 J *Ldlr*$^{-/-}$*-p16-Cre*^{ERT2}*-tdTomato* mice were generated by crossing C57BL/6 J *Ldlr*$^{-/-}$ mice with C57BL/6 J *p16-Cre*^{ERT2}*-tdTomato* mice (Omori et al., 2020). Experimental mice were homozygous for the *Ldlr*-knockout allele (*Ldlr*$^{-/-}$) and heterozygous for the *p16-Cre*^{ERT2} allele and the *tdTomato* allele. Unless otherwise specified, age-matched female mice were used for all experiments as female *Ldlr*$^{-/-}$ mice are more susceptible to the development of atherosclerosis (Daugherty et al., 2017). Mice were housed in a light- and temperature-controlled facility (21 °C) with *ad libitum* access to water and standard chow (Sniff, Germany) or high-fat high-cholesterol (HFC) diet (40% of kcal from fat, 0.15% cholesterol, Research Diets, D12079B, New Brunswick, NJ, US). Mice used for the chow experiments were housed in groups, whereas mice used for the HFC-diet experiment were housed individually to assess food intake. All animal experiments were approved by the Ethical Committee for Animal Experiments of the University of Groningen and were performed in accordance with relevant guidelines and regulations (including laboratory and biosafety regulations).

2.2. Animal experiments

Ldlr$^{-/-}$*-p16-3MR* mice were kept on standard chow diet until 8–10 weeks of age after which they received weekly intraperitoneal injections (i.p.) with 2.5 mg/kg of DOX hydrochloride (in phosphate-buffered saline (PBS), Tebu-Bio) or vehicle (PBS) for 4 weeks with a total cumulative dose of 10 mg/kg, unless otherwise specified. This DOX treatment regimen was chosen based on previous studies showing that administration of 2–10 mg/kg DOX resulted in toxicity in male and female mice, including impaired heart function, adipocyte insulin resistance, ovarian toxicity, and p16^{Ink4a+}-senescent cell accumulation (Vergoni et al., 2016; Biondo et al., 2018; Demaria et al., 2017; Pecoraro et al., 2016; dos Silva et al., 2023; Wang et al., 2019). Furthermore, a cumulative dosage of 10 mg/kg DOX is equivalent to 30 mg/m^2 (Reagan-Shaw et al., 2008), which is a relevant dosage in human clinical settings where cancer patients receive 15–90 mg/m^2 DOX (Quagliariello et al., 2021; Sedeman et al., 2022). Mice were randomly assigned to experimental groups. After DOX administration, *Ldlr*$^{-/-}$*-p16-3MR* mice were enrolled in different experimental designs. To determine the acute effects of DOX, *Ldlr*$^{-/-}$*-p16-3MR* mice were anesthetized using isoflurane (TEVA Pharmachemie), euthanized by cardiac puncture followed by cervical dislocation, and metabolic tissues were weighed and collected 1 week after the last DOX injection. Tissues for mRNA expression analysis were snap-frozen in liquid nitrogen and stored at −80 °C until further analysis. For heart function measurements, *Ldlr*$^{-/-}$*-p16-3MR* mice were kept for 6 additional weeks on chow until echocardiography was performed. To assess the effect of DOX on long-term cardiometabolic health, *Ldlr*$^{-/-}$*-p16-3MR* mice were treated with HFC-diet for 12 weeks, starting 7 days after the last DOX injection. Together with the start of the HFC-diet, one group of mice received GCV (in H20, Selleckchem, Germany) through i.p. injection for 5 consecutive days at a dose of 25 mg/kg to genetically eliminate p16^{Ink4a+}-cells. GCV was administered biweekly for in total 4 cycles of 5 days. After 12 weeks of HFC-diet, mice were fasted for 4–6 h and euthanized as described above. To investigate the induction of cellular senescence by DOX treatment, two additional experimental groups of *Ldlr*$^{-/-}$*-p16-3MR* mice were included that received 1 × 10 mg/kg DOX or 3 × 5 mg/kg DOX (consecutive days) through i.p. injection. Tissues for mRNA expression analysis were collected 1 week after the last DOX treatment as described above. *Ldlr*$^{-/-}$*-p16-Cre*^{ERT2}*-tdTomato* mice were kept on chow diet and received 4 × 2.5 mg/kg DOX (weekly interval) or 1 × 10 mg/kg DOX through i.p. injection at 8–10 weeks of age. Starting 7 days after the last DOX injection, *Ldlr*$^{-/-}$*-p16-Cre*^{ERT2}*-tdTomato* mice were treated with a daily i.p. injection of tamoxifen (TAM, 80 mg/kg in sunflower oil, Sigma Aldrich, St. Louis, MO, US) for 5 consecutive days to label p16^{Ink4a}-expressing cells with tdTomato (TOM). One week later, mice were terminated under isoflurane anesthesia and tissues were collected to measure percentage of TOM-positive (TOM$^+$) cells by immunofluorescence imaging.

2.3. Echocardiography

Transthoracic echocardiography was performed using a Vevo imaging station and a Vevo 3100 preclinical imaging system (FUJIFILM VisualSonics, Canada), equipped with a 40-MHz MX550D linear array transducer (FUJIFILM VisualSonics). Prior to echocardiographic imaging, mice were anesthetized (2% isoflurane mixed with oxygen, administered *via* an aerial dispenser) and fur was removed from the thorax using a commercially available topical depilation agent with potassium thioglycolate (Veet). Mice were fixed in supine position on the temperature-maintained (37 °C) platform of the Vevo imaging station (FUJIFILM VisualSonics) over the integrated electrode pads to monitor heart and respiration rates. Vevo LAB software (version 5.6.1, FUJIFILM VisualSonics) was used for image analysis. Short axis M-mode recordings were used to determine heart rate, left ventricular (LV) end-diastolic internal diameter, LV end-systolic internal diameter, and fractional shortening by outlining the epicardial and endocardial borders using the LV Trace tool. For all measurements, three subsequent cardiac cycles unaffected by respiration were analyzed.

2.4. Analysis of glucose homeostasis

To determine the effect of DOX on glucose homeostasis, an oral glucose tolerance test (oGTT) was performed on *Ldlr*$^{-/-}$*-p16-3MR* mice after 9 weeks of HFC-diet. For the oGTT, 10-h overnight fasted mice received an oral gavage of 1.5 g/kg glucose. Blood glucose levels were measured at baseline and 15, 30, 60, 90, and 120 min after glucose administration using an Accu-Chek Performa glucose meter (Roche Diabetes Care). During the oGTT, blood spots were collected on filter paper (Sartorius Stedim, TFN 180 g·m^{-2}, Germany) at baseline and 15 min after glucose administration to determine insulin levels. Insulin was extracted from blood spots and measured by ELISA (Crystal Chem Rat Insulin Elisa Cat. 90,010 with mouse insulin standard Cat.90020) according to the manufacturer's instructions. To assess insulin sensitivity, an insulin tolerance test (ITT) was performed on *Ldlr*$^{-/-}$*-p16-3MR* mice after 11 weeks of HFC-diet. After a 5-h fast, mice received an i.p. injection of 0.5 unit(U)/kg insulin (Novorapid, Novo Nordisk, Denmark). Blood glucose levels were measured at baseline and 15, 30, 60, 90, and 120 min after insulin injection. After 10 weeks of HFC-diet, body composition of *Ldlr*$^{-/-}$*-p16-3MR* mice was determined using a Minispec Body Composition Analyzer (LF90; Bruker Daltonics, Billerica, MA, US).

2.5. Gene expression analysis

For gene expression analysis, aortas were enzymatically digested with liberase TH (Roche), hyaluronidase (Sigma-Aldrich), and DNase (Sigma-Aldrich) for 30 min at 37 °C. Subsequently, cold PBS was added and samples were centrifuged at 4 °C for 10 min at 15.000 rcf. The pellet was resuspended in RLT Buffer (Qiagen) and RNA was isolated using the RNeasy mini kit (Qiagen). For liver and heart tissues, total RNA was isolated using TRI reagent (Sigma-Aldrich). Total RNA from adipose tissue was isolated using an RNeasy Lipid Tissue Mini Kit (Qiagen). RNA was reverse transcribed using Moloney-Murine Leukemia Virus reverse transcriptase (Thermo Fisher Scientific) and transcript levels of synthesized cDNA were measured with Fast Start SYBR Green (Roche) on a Quantstudio 7 Flex Real-time PCR System (Applied Biosystems). Gene expression levels were quantified by the relative standard curve method and normalized to a housekeeping gene (*36b4* for adipose tissue, heart, and aorta, *Cyclophilin* for liver). qPCR primer sequences are listed in Table S1.

2.6. Analysis of blood and plasma parameters

After 12 weeks of HFC-diet, blood was drawn from 4 to 6-h fasted mice by cardiac puncture under isoflurane anesthesia, collected into EDTA-coated tubes (Sarstedt, Germany), and plasma was separated by centrifugation. Circulating levels of alanine aminotransferase (ALT) and aspartate aminotransferase (AST) in plasma were measured by a routine clinical chemistry analyzer (Cobas 6000; Roche Diagnostics) with standard reagents (Roche Diagnostics). Plasma triglycerides (Roche Diagnostics #1187771) and total cholesterol (DiaSys Diagnostic Systems) were measured using commercially available kits. To determine whether DOX affected hematological parameters, blood was collected before the start of the HFC-diet and after 5 and 9 weeks of HFC-diet. Blood was taken through the tail vein and collected in heparin-coated capillaries. Per animal, 25 μl of whole blood was diluted in 5 ml sample diluent (Medonic CA 620, Clinical Diagnostic Solutions) and measured using the Medonic CA620 (Medicon, Ireland).

2.7. Hepatic lipid content

To determine hepatic lipid content, liver homogenates (15% wt/vol in PBS) were subjected to lipid extraction as described by Bligh & Dyer (Bligh and Dyer, 1959). For assessment of hepatic triglyceride levels, extracts were diluted in 2% Triton-x-100 and measured using a Trig/GB kit (Roche Diagnostics #1187771). Total cholesterol levels were determined using a colorimetric assay (DiaSys Diagnostic Systems).

2.8. Histological analysis

For histological analysis, tissues were isolated and fixed using 4% formaldehyde solution in phosphate buffer (Klinipath BV). After fixation, tissues were dehydrated, embedded in paraffin, and cut into 4-μm sections. Slides were subjected to hematoxylin-eosin (H&E) staining and were imaged using a Hamamatsu NanoZoomer (Hamamatsu Photonics). Adipocyte area was quantified by randomly counting >150 adipocytes per mouse using ImageJ (NIH). Cells <350 μm were excluded as they could be stromal vascular cells. Number of crown-like structures (CLS) were calculated as average of three microscopic fields per animal. To detect TOM expression, immunofluorescence staining was performed using a primary antibody against RFP (Abcam, ab124754) and a secondary antibody conjugated to Alexa Fluor™ 488 (Invitrogen, #A11008). Slides were scanned using the SLIDEVIEW VS200 slide scanner (Olympus) and imaged using OlyVIA software (version 3.4.1, Olympus). TOM^{+}-cells were quantified using ImageJ software and normalized to total number of DAPI-positive cells on two randomly selected fields (3000 μm × 1500 μm) per animal per tissue.

2.9. Atherosclerotic lesion analysis

Atherosclerotic lesion analysis was performed on 4-μm H&*E*-stained cross sections of the aortic root area of the heart. For each animal, morphometric analysis of the valves was performed on five evenly spaced sections (40 μm separation) using Aperio ImageScope Software (Leica Biosystems, Pathology) in a blinded manner. Average plaque size per animal was calculated as the sum of the plaque size of three valves. Necrotic core area was identified as acellular area, lacking nuclei and cytoplasm, and quantification of the necrotic core was performed using Aperio ImageScope Software as previously described with a threshold of 3000 μm^2 (Seimon et al., 2009). Necrotic core area is presented as μm^2 area per animal. Fibrous cap thickness was measured by choosing the largest necrotic core from serial sections (40 μm apart). Using Aperio ImageScope, two measurements (2 μm apart) were taken from the thinnest part of the cap, determined by measuring the area between the outer edge of the cap and the necrotic core boundary, as previously described (Seimon et al., 2009). Per animal, the average fibrous cap thickness was expressed in length units (μm).

2.10. Statistical analysis

Statistical analysis was performed using Graphpad Prism Software version 9.5.0 (GraphPad Software, San Diego, CA, US). Differences

between two groups were analyzed using an unpaired 2-tailed Student's *t-test*. Multiple comparisons were tested using a one-way ANOVA followed by Tukey's multiple comparisons test. A repeated measurement two-way ANOVA followed by a Bonferroni's *post hoc* test was used to evaluate glucose tolerance, insulin tolerance, and body weight in time. Data are presented as mean ± standard error of the mean (SEM) with a p value <0.05 considered significant.

3. Results

3.1. Acute toxicity of doxorubicin in $Ldlr^{-/-}$-p16-3MR mice

The cell-cycle inhibitor $p16^{Ink4a}$ has been generally used as senescence marker in human and mouse tissues (He and Sharpless, 2017). The *p16-3MR* mouse model, in which $p16^{Ink4a+}$-senescent cells can be visualized and genetically eliminated upon administration of ganciclovir (GCV), has been widely used in studies investigating the role of senescent cells in ageing and age-related diseases (Demaria et al., 2014). Using this mouse model, a causal role for $p16^{Ink4a+}$-senescent cells has been demonstrated for various DOX-induced side effects, including cardiac and arterial dysfunction, increased blood clotting, frailty, and tumor recurrence (Demaria et al., 2017; Wiley et al., 2019; Hutton et al., 2021). Therefore, to study the effect of DOX on senescence and cardiometabolic disease development, we crossed atherosclerosis-prone $Ldlr^{-/-}$ mice with *p16-3MR* mice. First, we assessed the acute toxic effects of four weekly injections of 2.5 mg/kg DOX in chow-fed $Ldlr^{-/-}$-*p16-3MR* mice (Fig. 1A). As expected, body weight as well as gonadal white adipose tissue (gWAT) weight were significantly reduced in DOX-treated mice, whereas mesenteric white adipose tissue (mWAT) and subcutaneous adipose tissue (scWAT) depots were not affected (Fig. 1B, C). Furthermore, we found a reduction in circulating white blood cells (WBCs), specifically in the lymphocyte population, which is also a common side-effect of chemotherapeutic treatment (Fig. 1D). Together, these results are in line with the known acute effects of DOX and thus indicate that our DOX treatment was effective.

As the effect of DOX was most prominent in gWAT, we further analyzed this tissue for effects on inflammation and senescence. While one week after DOX treatment no difference was observed in adipocyte size, a significantly increased number of crown-like structures (CLS) was observed in DOX-treated mice, indicating increased adipose inflammation (Fig. 1E-G). Induction of adipose inflammation was further confirmed by increased gene expression of *Tnf, Cxcl10,* and *Mmp13* (Fig. 1H). Interestingly, we also found an increase in the cell-cycle inhibitor and p53-target gene *p21* in gWAT. The *p21* gene controls cell-cycle progression in response to various stressors, including DNA damage (Karimian et al., 2016) and has, in addition to $p16^{Ink4a}$, recently been recognized as marker and major regulator of cellular senescence (Wang et al., 2021). In contrast to *p21*, expression of $p16^{Ink4a}$ was not induced by DOX treatment. Furthermore, DOX treatment did not result in decreased expression of lamin B1 (*Lmnb1*), another biomarker of

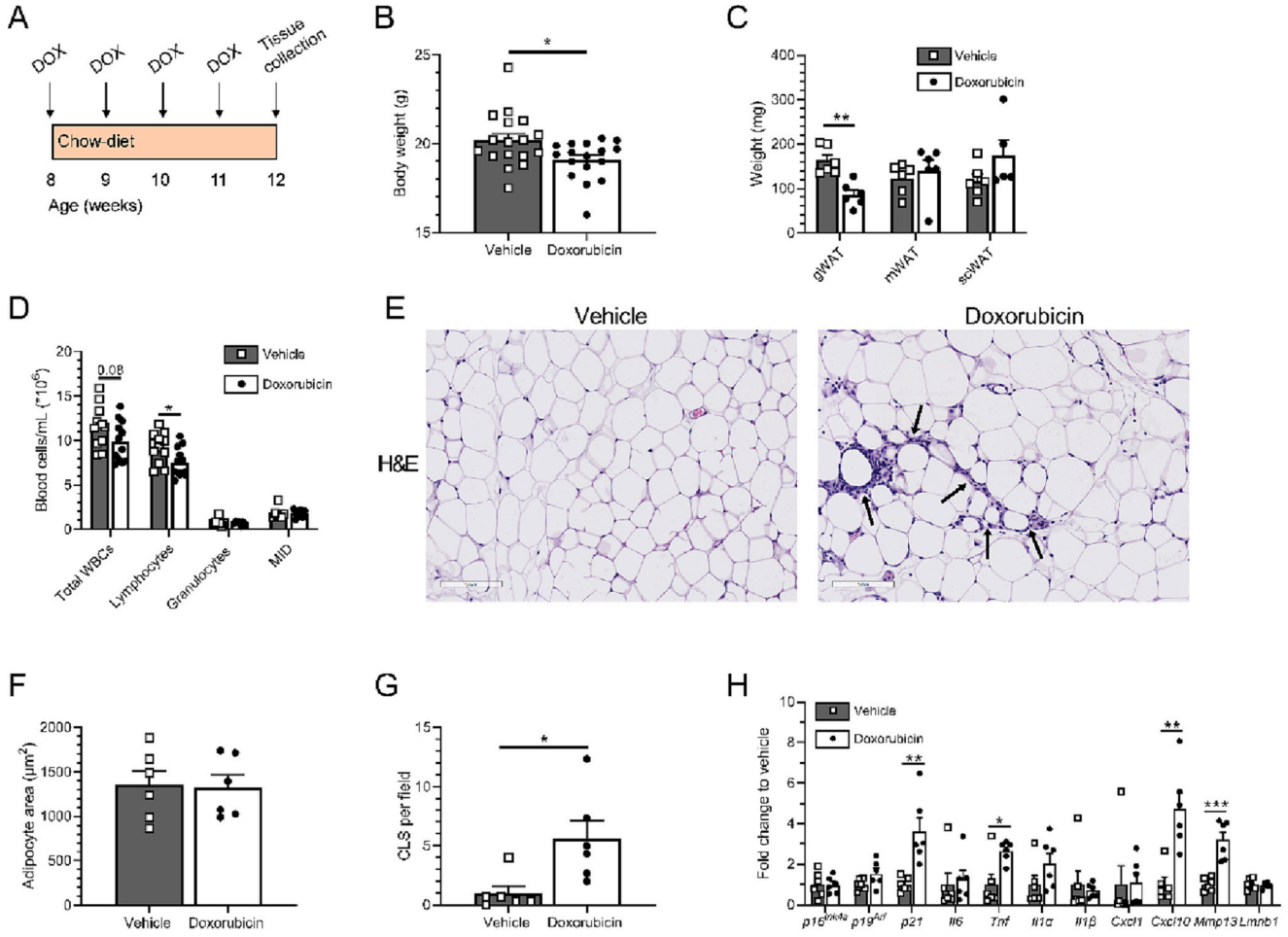

Fig. 1. Acute toxicity of DOX in $Ldlr^{-/-}$-*p16-3MR* mice. (A) Experimental timeline of the chow experiment in which $Ldlr^{-/-}$-*p16-3MR* mice received 4 weekly injections of 2.5 mg/kg DOX or vehicle. (B) Body weight ($n = 17$), (C) weights of different white adipose tissue depots ($n = 5$–6), and (D) white blood cell (WBC) counts 1 week after DOX treatment ($n = 7$–12). MID = mid-range other WBCs. (E) Representative H&*E*-stained images of gWAT, (F) corresponding quantification of adipocyte area, and (G) average number of crown-like structures (CLS) (indicated by arrows) per field 1 week after DOX treatment ($n = 6$). (H) Gene expression of senescence and SASP-markers in gWAT 1 week after DOX treatment (n = 6). Data are presented as mean ± SEM with * $p < 0.05$, ** $p < 0.01$, and *** $p < 0.001$.

senescence (Freund et al., 2012). Other tissues examined (liver, heart, and aorta) did not show significant induction of senescence or SASP-markers upon DOX treatment (Fig. S1A-C). Overall, DOX treatment induced acute gWAT inflammation and *p21* expression, which could indicate senescent cell accumulation, but not $p16^{Ink4a}$ expression.

3.2. Long-term effects of doxorubicin treatment on gonadal white adipose tissue

To investigate the long-term effects of DOX on induction of cellular senescence and the development of cardiometabolic disease, we induced metabolic stress by feeding $Ldlr^{-/-}$*-p16-3MR* mice a high-fat high-cholesterol (HFC) diet for 12 weeks (Fig. 2A). No effect of DOX was

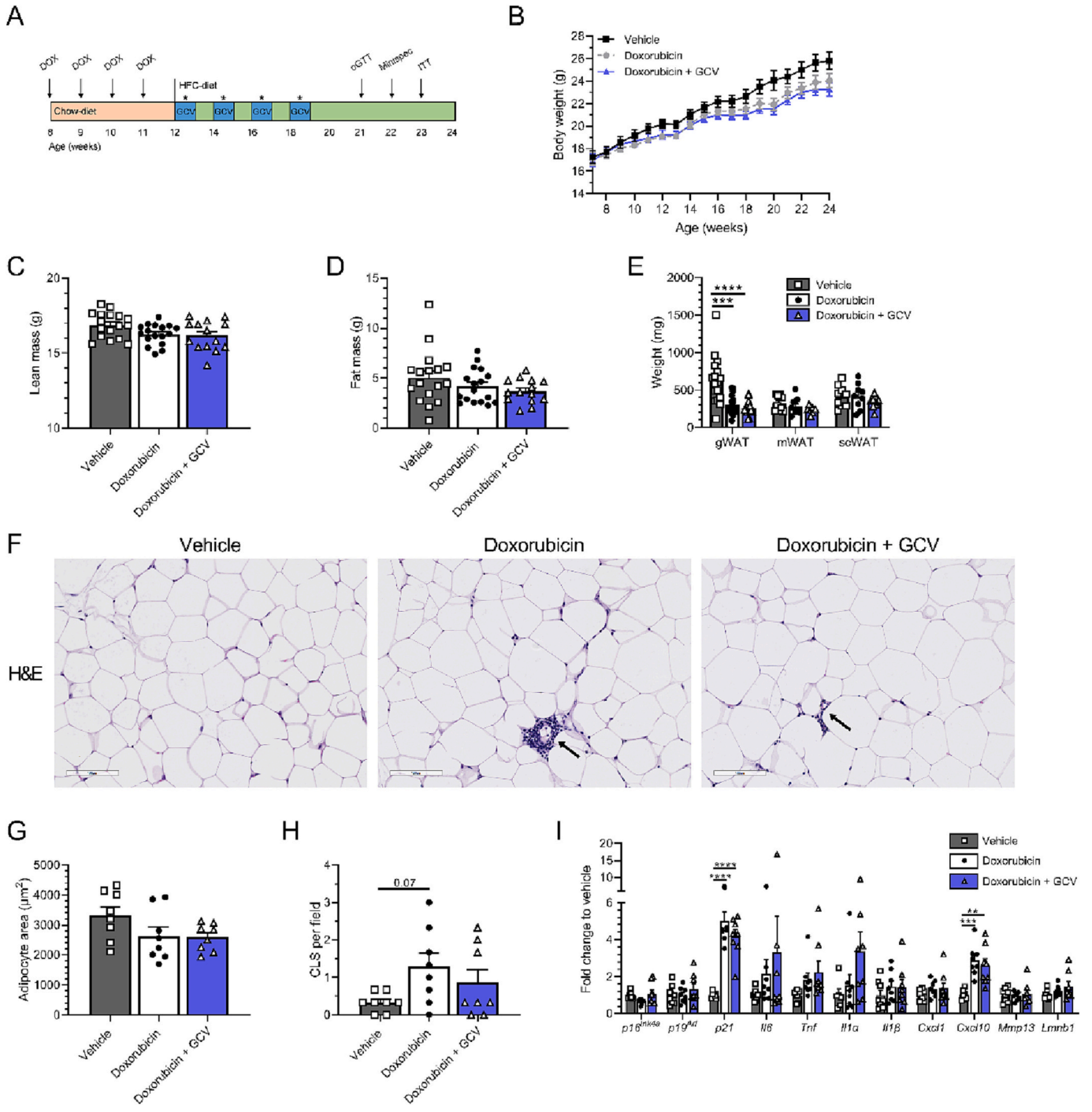

Fig. 2. Long-term effects of DOX treatment on gonadal white adipose tissue in $Ldlr^{-/-}$*-p16-3MR* mice. (A) Experimental timeline of the HFC-diet experiment in which $Ldlr^{-/-}$*-p16-3MR* mice received 4 weekly injections of 2.5 mg/kg DOX or vehicle followed by 12 weeks of HFC-diet feeding. A third experimental group received GCV following DOX treatment to clear $p16^{Ink4a+}$-senescent cells. * indicates 5 consecutive days of GCV treatment. (B) Body weight during DOX treatment and 12 weeks of HFC-diet feeding ($n = 14$–17). (C) Lean mass and (D) fat mass after 10 weeks of HFC-diet feeding (n = 14–17). (E) Weights of different white adipose tissue depots after 12 weeks of HFC-diet feeding ($n = 8$–17). (F) Representative H&*E*-stained images of gWAT, (G) corresponding quantification of adipocyte area, and (H) average number of CLS (indicated by arrows) (n = 8). (I) Gene expression of senescence markers in gWAT (n = 8). Data are presented as mean ± SEM with * $p < 0.05$, ** $p < 0.01$, *** $p < 0.001$ and **** $p < 0.0001$.

observed on body weight, body composition, or food intake (Fig. 2B-D, S2). The reduction in gWAT weight that was observed acutely after DOX treatment, however, was still present in mice fed a 12-week HFC-diet and there was still a trend towards an increase in the number of CLS (Fig. 2E-H). Gene expression of *p21* and *Cxcl10* remained significantly elevated in gWAT long-term after DOX treatment, while other senescence and SASP-factors were not altered (Fig. 2I). These findings suggest that while DOX treatment induced a long-term reduction in gWAT mass and increase in *p21* expression, which could indicate accumulation of $p21^{+}$-senescent cells, these effects were not associated with an accumulation of $p16^{Ink4a+}$-senescent cells.

Transplantation studies have shown that only a small number of senescent cells (0.01% to 0.03%) throughout the body is already sufficient to cause physical dysfunction in young mice (Xu et al., 2018). DOX treatment could therefore have physiological consequences by inducing a small number of $p16^{Ink4a+}$-senescent cells, which we were not able to detect by qPCR in whole tissue homogenates. To exclude that undetected $p16^{Ink4a+}$-senescent cells play a role in the effects of DOX on the gWAT depot, we treated mice with GCV following DOX administration to eliminate $p16^{Ink4a+}$-senescent cells (Fig. 2A). However, removal of $p16^{Ink4a+}$-senescent cells did not restore gWAT weight (Fig. 2E) or reduce the expression of *p21* or *Cxcl10* (Fig. 2I), suggesting that the effect of DOX on gWAT is not mediated through $p16^{Ink4a+}$-senescent cells nor is reversible.

3.3. Long-term effects of doxorubicin treatment on glucose homeostasis

Adipose tissue plays a central role in whole-body glucose homeostasis (Luo and Liu, 2016). Since DOX had a significant effect on gWAT, the adipose depot most strongly linked to insulin resistance, we determined whether this also had an effect on glucose homeostasis in response to HFC-diet. No effect of DOX, however, was observed on random or fasted glucose levels, glucose tolerance (oGTT), fasted insulin levels, glucose-stimulated-insulin-secretion after an oral glucose bolus, and insulin sensitivity (ITT) (Fig. 3A-E). In line with the gWAT data, clearance of $p16^{Ink4a+}$-senescent cells did not improve glucose tolerance and insulin sensitivity in HFC-diet fed animals, except that a slightly lower blood glucose level was observed at the end of the ITT as compared to control mice (Fig. 3A-E). Together, these data show that DOX treatment has no significant long-term effects on whole-body glucose homeostasis and that this was also not affected by clearance of $p16^{Ink4a+}$-cells in this mouse model.

3.4. Long-term effects of doxorubicin treatment on liver

Next, we determined the effect of DOX on steatosis, inflammation, and damage of the liver in response to an HFC-diet. DOX did not affect liver weight, liver to body weight ratio, and hepatic levels of total cholesterol and triglycerides (Fig. 4A-E). Plasma ALT levels were significantly lower in DOX-treated mice compared to control mice, whereas plasma AST levels were similar between the groups, indicating that liver damage was not increased, or maybe even reduced (Fig. 4F, G). Senescence and SASP-markers were not changed after 12 weeks of HFC-diet feeding (Fig. 4H). Removal of $p16^{Ink4a+}$-senescent cells did reduce liver weight, however not after correction for body weight, hepatic triglyceride levels, and hepatic *Mmp13* expression compared to HFC-diet fed control mice, but not to DOX-treated mice (Fig. 4A, B, E, H). Overall, these findings indicate that DOX does not have a significant effect on

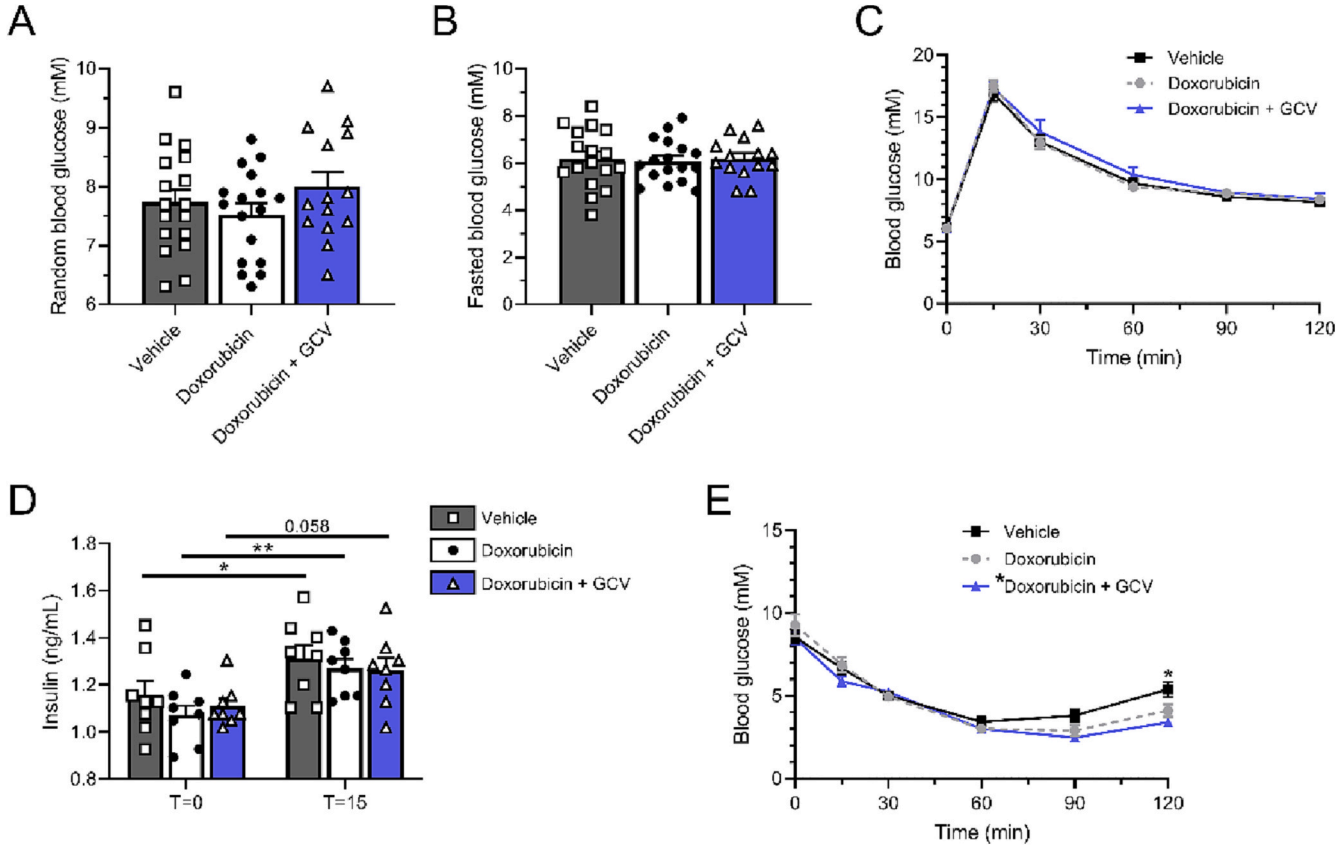

Fig. 3. Long-term effects of DOX on glucose homeostasis in *Ldlr*$^{-/-}$*-p16-3MR* mice. Measurements of glucose homeostasis were performed according to the timeline in Fig. 2A. (A) Random blood glucose levels after 12 weeks of HFC-diet feeding (n = 14–17). (B) 10-h overnight fasted blood glucose levels (n = 14–17), (C) blood glucose levels during the oGTT (n = 14–17), and (D) whole-blood insulin levels at baseline and T = 15 min of the oGTT (n = 8) after 9 weeks of HFC-diet feeding. (E) Blood glucose levels during the ITT after 11-weeks of HFC-diet feeding, * indicates significance compared to vehicle (n = 8–10). Data are presented as mean ± SEM with * $p < 0.05$ and ** $p < 0.01$.

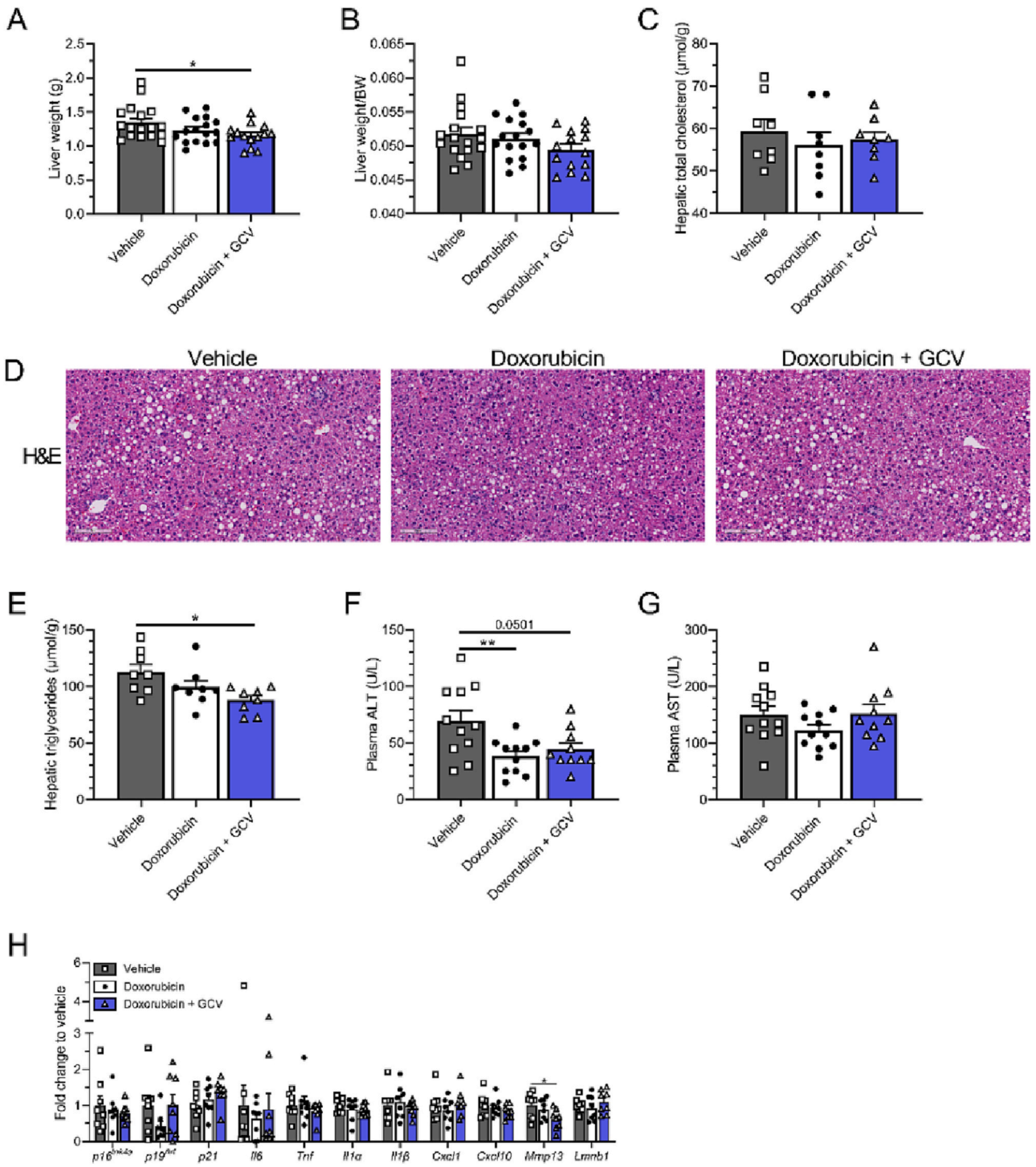

Fig. 4. Long-term effects of DOX treatment on liver in *Ldlr*$^{-/-}$*-p16-3MR* mice. (A) Liver weight and (B) liver weight to body weight ratio ($n = 14$–17) after 12 weeks of HFC-diet feeding. (C) Hepatic total cholesterol content, (D) representative H&*E*-stained images of livers from vehicle-, DOX-, and DOX + GCV-treated mice, and (E) hepatic triglyceride content after 12 weeks of HFC-diet feeding ($n = 8$). (F) ALT and (G) AST levels in 4-h fasted plasma samples after 12 weeks of HFC-diet feeding ($n = 10$–11). (H) Relative mRNA expression of senescence and SASP-markers in liver tissue after 12 weeks of HFC-diet feeding (n = 8). Experiments were performed according to the experimental timeline in Fig. 2A. Data are presented as mean ± SEM with * $p < 0.05$ and ** $p < 0.01$.

hepatic steatosis, inflammation, or damage.

3.5. Long-term effects of doxorubicin treatment on heart function

Cardiotoxicity is one of the most common toxic side effects of DOX (Volkova and Russell, 2011). At six weeks after the last DOX injection, however, mice on chow showed normal heart rate and did not display reduced ejection fraction or fractional shortening as determined by echocardiography (Fig. 5A-D). In addition, no effect of DOX was observed on heart weight and morphology (Table 1). At 12 weeks after HFC-diet feeding, expression levels of *p16*^{Ink4a} and *p21* were not increased and no changes were observed in the expression of *Nppa*, which encodes atrial natriuretic peptide (ANP), a cardiac hormone and biomarker for heart failure (Song et al., 2015), and of *Col1a1*, a marker

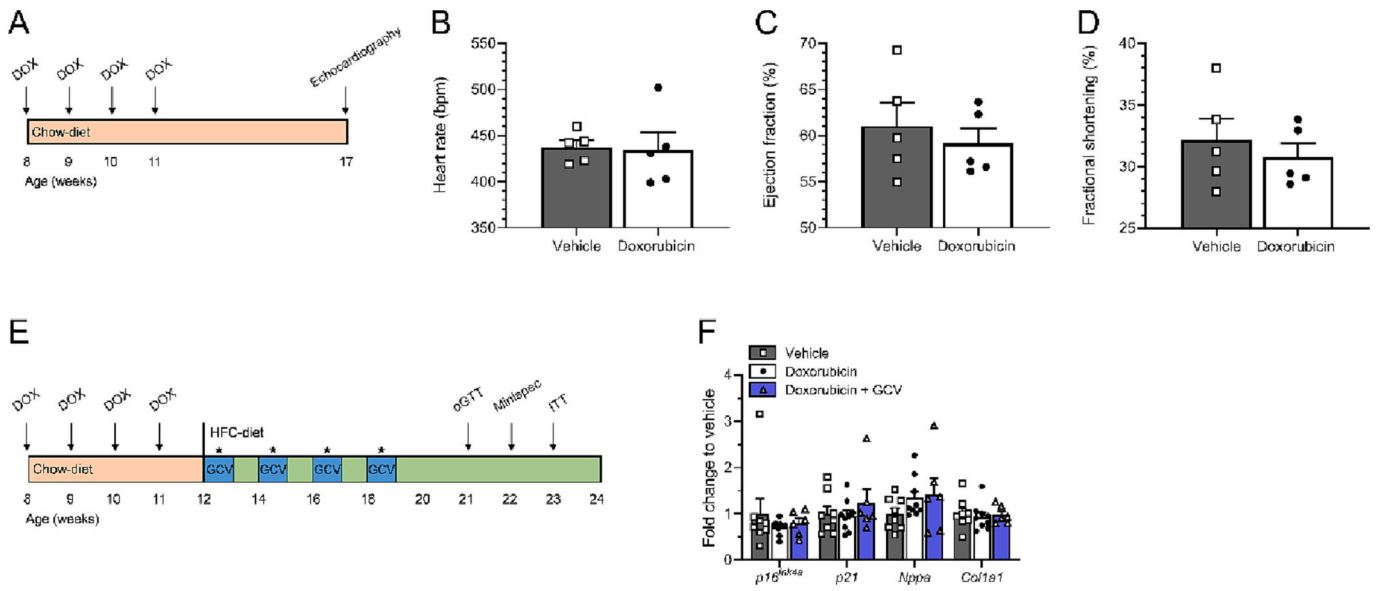

Fig. 5. Long-term effects of DOX treatment on heart function in *Ldlr*$^{-/-}$*-p16-3MR* mice. (A) Experimental timeline of the experiment in which heart function was assessed. *Ldlr*$^{-/-}$*-p16-3MR* mice received 4 weekly injections of 2.5 mg/kg DOX or vehicle followed by echocardiography 6 weeks after the last DOX injection by which (B) heart rate, (C) ejection fraction, and (D) fractional shortening were measured ($n = 5$). (E) Experimental timeline of the results depicted in (F), * indicates 5 consecutive days of GCV treatment. (F) For gene expression analysis of relevant markers heart tissues were collected after 12 weeks of HFC-diet feeding ($n = 6$–9). Data are presented as mean ± SEM.

Table 1
Cardiac parameters in chow-fed *Ldlr*$^{-/-}$*-p16-3MR* mice 6 weeks after DOX treatment.

Parameter	Vehicle	Doxorubicin
Heart weight/tibia length (mg/mm)	7.0 ± 0.2	7.4 ± 0.3
Stroke volume (μl)	34.1 ± 0.7	33.7 ± 1.4
End-systolic volume (μl)	22.1 ± 2.3	23.3 ± 1.3
End-diastolic volume (μl)	56.2 ± 2.5	56.9 ± 2.0
Diastolic diameter (mm)	3.65 ± 0.07	3.67 ± 0.05
Systolic diameter (mm)	2.48 ± 0.11	2.54 ± 0.06
Diastolic anterior wall (mm)	0.84 ± 0.03	0.86 ± 0.03
Systolic anterior wall (mm)	1.24 ± 0.03	1.19 ± 0.01
Diastolic posterior wall (mm)	0.79 ± 0.04	0.74 ± 0.02
Systolic posterior wall (mm)	1.11 ± 0.02	1.06 ± 0.01

of cardiac fibrosis (Fig. 5E, F). In conclusion, we did not find evidence for impaired cardiac function or induced cardiac senescence after four cycles of low-dose DOX in *Ldlr*$^{-/-}$*-p16-3MR* mice.

3.6. Long-term effects of doxorubicin treatment on atherosclerotic plaque size and stability

Children and adolescents who have been treated with DOX are not only at risk to develop heart failure, but also of developing severe vascular disease later in life (Mitry and Edwards, 2016). The vascular endothelium, consisting of a monolayer of endothelial cells lining the vessel wall, can be disrupted by DOX, which can trigger the onset of atherosclerosis, especially in a hyperlipidemic environment (Luu et al., 2018). Although *Ldlr*$^{-/-}$*-p16-3MR* mice displayed considerable atherosclerotic plaque development in response to the HFC-diet, no effect was observed of DOX on atherosclerotic lesion size in the aortic root (Fig. 6A, B, S3). Atherosclerosis development is also importantly influenced by circulating monocytes as they infiltrate into the vessel wall and become lipid-laden macrophages (Moore et al., 2013). Because acute exposure to DOX resulted in myelosuppression (Fig. 1D), we also measured blood cell counts after 5 and 9 weeks of HFC-diet feeding. Total WBC counts as well as different WBC subpopulations, including monocytes, however, were normal again at 5 weeks after DOX treatment and remained similar to control mice throughout the course of the study (Table S2). Furthermore, plasma levels of cholesterol and triglycerides, the main drivers of atherosclerosis, were not different between the experimental groups (Fig. 6C, D).

Unstable plaques are vulnerable to spontaneous rupture, causing acute thrombosis, arterial occlusion, and infarction (Childs et al., 2021). Therefore, we questioned whether DOX affected plaque stability. However, necrotic core size as well as fibrous cap thickness were not changed upon DOX treatment (Fig. 6E, F). To determine whether the aortic arch showed signs of senescence that could predispose for future plaque instability, we measured gene expression of relevant markers. However, DOX treatment did not affect expression levels of *p16*^{Ink4a}, *p21*, *Tnf*, or *Il1α* after 12 weeks of HFC-diet feeding (Fig. 6G). Finally, clearance of p16^{Ink4a+}-senescent cells did not affect atherosclerotic lesion size or stability between vehicle- and DOX-treated mice (Fig. 6A, B, E, F). Together, these results indicate that DOX treatment does not affect size and stability of atherosclerotic plaques and that atherosclerosis development was also not affected by clearance of p16^{Ink4a+}-cells in this mouse model.

3.7. Different doxorubicin treatment regimens do not induce p16^{Ink4a+}-senescent cell accumulation in two independent mouse models

As administration of 4 × 2.5 mg/kg DOX did not result in a significant senescence induction in metabolic tissues, except for increased expression of *p21* and a few SASP-factors in gWAT, we wondered whether higher DOX treatment regimens that have been reported in the literature to induce p16^{Ink4a+}-senescent cell accumulation, could also induce senescence in our *Ldlr*$^{-/-}$*-p16-3MR* mouse model (Demaria et al., 2017; Wang et al., 2022a). However, we did not observe an effect of these higher DOX regimens on levels of *p16*^{Ink4a} or SASP-factors in liver or gWAT (Fig. 7A-C). Only *p21* showed a dose-dependent increase with a significant higher expression in 3 × 5 mg/kg DOX-treated mice compared to controls. In gWAT, *p21* and *Cxcl10* were increased to the same extent in the 3 × 5 mg/kg and 4 × 2.5 mg/kg DOX groups, whereas the 1 × 10 mg/kg DOX group showed a similar trend but did only reach statistical significance for *Il1α* (Fig. 7C). Similarly, heart tissue of none of the DOX-treated groups showed differences in the expression of *p16*^{Ink4a},

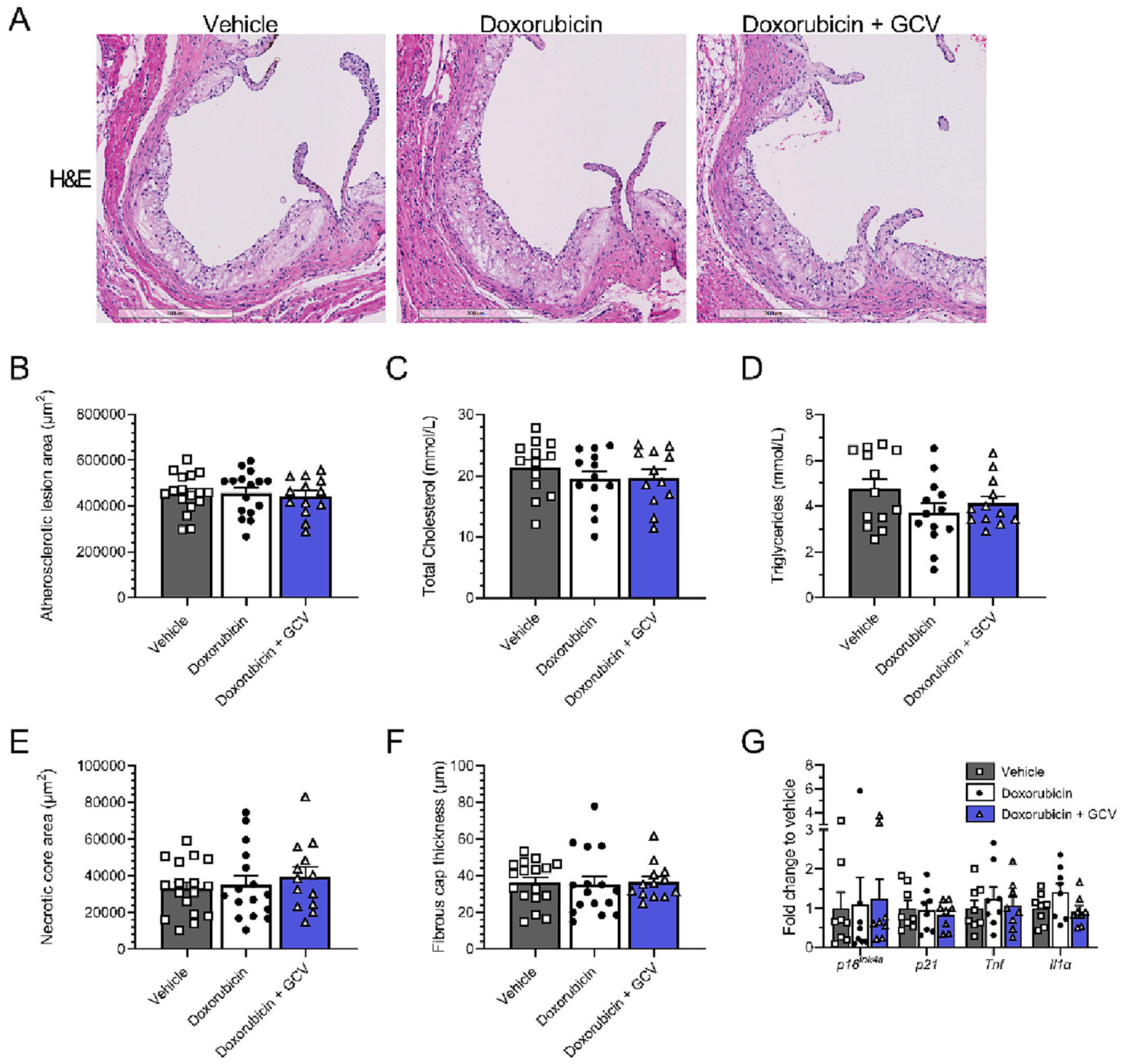

Fig. 6. Long-term effects of DOX treatment on atherosclerotic plaque size and stability in *Ldlr*$^{-/-}$*-p16-3MR* mice. (A) Representative images of H&*E*-stained atherosclerotic plaques in the aortic root area of the heart and (B) corresponding quantification of atherosclerotic lesion area after 12 weeks of HFC-diet feeding (n = 13–17). (C) Plasma total cholesterol and (D) plasma triglycerides in 4-h fasted plasma samples after 12 weeks of HFC-diet feeding (n = 12–13). (E) Quantification of necrotic core area and (F) fibrous cap thickness of H&E-stained atherosclerotic plaques in (A). (G) Relative mRNA expression of senescence markers after 12 weeks of HFC-diet feeding (n = 8). Experiments were performed according to the experimental timeline depicted in Fig. 2A. Data are presented as mean ± SEM.

p21, *Nppa,* and *Col1a1* (Fig. 7D).

Because the lack of an induction of p16^{Ink4a+}-senescent cells upon DOX treatment could potentially be caused by the mouse model that we used, we also tested the effects of DOX in a different p16-reporter mouse model, the *Ldlr*$^{-/-}$*-p16-Cre*^{ERT2}*-tdTomato* model, which allows the labelling of p16^{Ink4a+}-cells with tdTomato (TOM) specifically in the presence of tamoxifen (TAM) [31, Fig. 8A]. Treatment, however, of this mouse model with 4 × 2.5 mg/kg or 1 × 10 mg/kg DOX followed by TAM treatment also did not increase the presence of p16^{Ink4a+}-cells (TOM^{+}-cells) in any of the examined organs (Fig. 8B-F). Together, these findings show that the used DOX treatment regimens did not exacerbate p16^{Ink4a+}-senescent cell accumulation in different tissues of two independent p16 reporter mouse models.

4. Discussion

Anthracycline-based chemotherapy has been associated with an increased risk of cardiometabolic disease later in life (de Haas et al., 2010; Dieli-Conwright et al., 2022). While the underlying mechanisms have not been identified, therapy-induced p16^{Ink4a+}-senescent cells have recently been proposed as a causal player (Demaria et al., 2017). Here, we show that four cycles of low-dose (2.5 mg/kg) DOX does not exacerbate p16^{Ink4a+}-senescent cell accumulation or development of cardiometabolic disease in metabolically stressed young adult female *Ldlr*$^{-/-}$*-p16-3MR* mice.

Treatment of *Ldlr*$^{-/-}$*-p16-3MR* mice with DOX resulted in an acute reduction in gWAT mass, which was accompanied by inflammation and

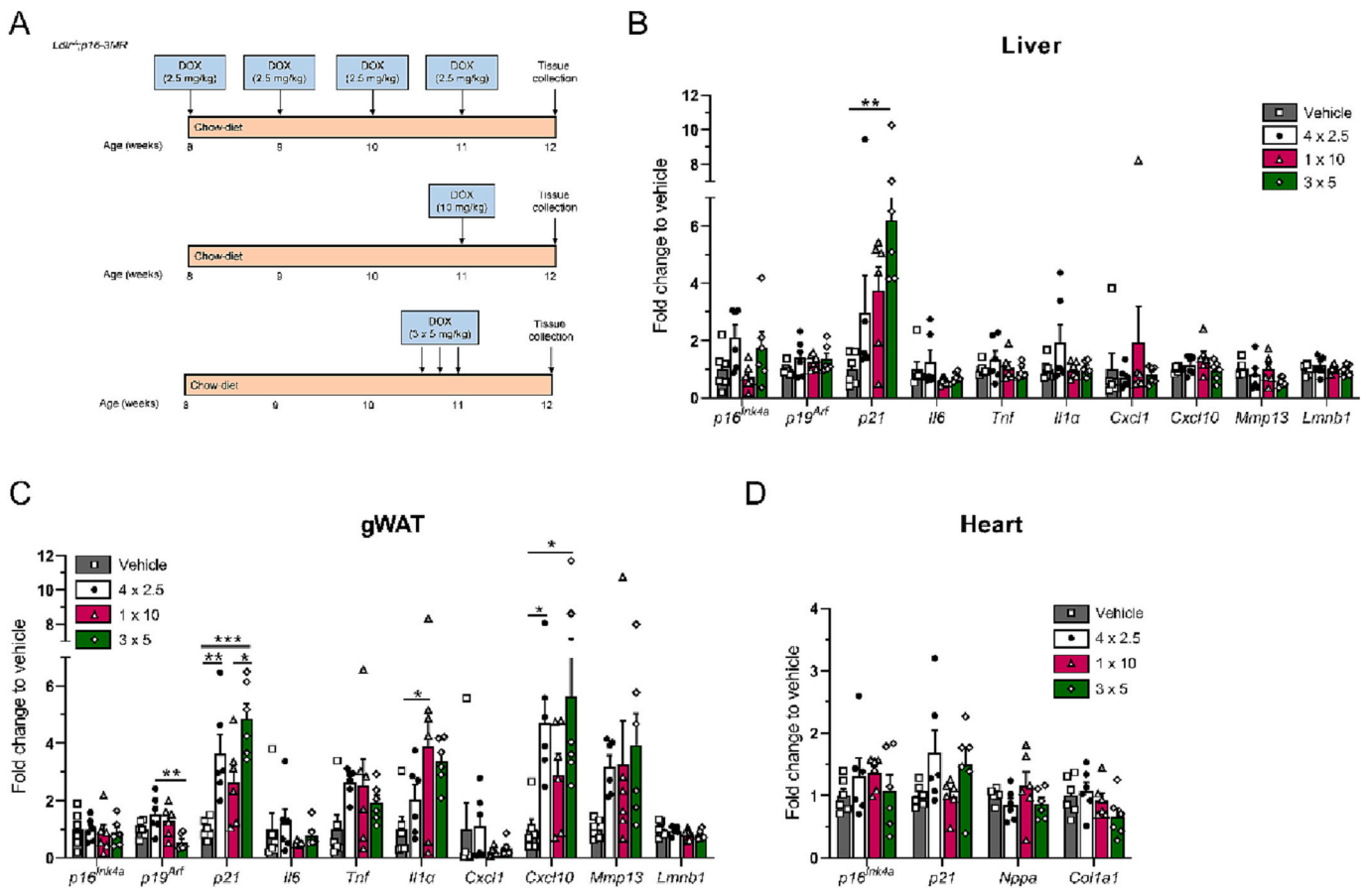

Fig. 7. Different DOX treatment regimens do not induce p16^{Ink4a+}-senescent cell accumulation in *Ldlr*$^{-/-}$*-p16-3MR* mice. (A) Experimental timeline of the different DOX treatment regimens in *Ldlr*$^{-/-}$*-p16-3MR* mice. Gene expression of senescence markers and other relevant markers in (B) liver, (C) gWAT, and (D) heart tissue ($n = 6$). Data are presented as mean ± SEM with * $p < 0.05$, ** $p < 0.01$ and *** $p < 0.001$.

increased expression of the senescence marker *p21*. Our findings are in line with previous experiments in rodents that have shown that DOX can impair adipose tissue function and metabolic homeostasis (Vergoni et al., 2016; Biondo et al., 2018; de Lima Junior et al., 2016). However, these studies only determined acute effects up till a few days after DOX administration, while, in human patients, perturbations in metabolic function can occur years after completion of treatment. Although the effects of DOX on gWAT in our study remained present after 3 months of HFC-diet feeding, we did not find any DOX-related long-term effects on metabolic health.

The finding that DOX treatment does not have long-term effects on cardiometabolic symptoms in our mouse model was unexpected as several human studies have reported that cancer survivors treated with anthracyclines have an increased risk of developing cardiometabolic disease (Baker et al., 2020; Clayton et al., 2021; Sharma et al., 2016; Shimizu et al., 2022). In line with human data, we observed acute toxicity of DOX in our mice, including effects on body weight, white blood cell count, and gonadal adipose tissue. Furthermore, the dosage of DOX used in this study was comparable to human patients, who receive 6–8 doses of DOX at 1.25 mg/kg (Demaria et al., 2017), suggesting that our findings cannot be explained by an insufficient treatment regimen. However, we cannot rule out that the biologically effective DOX dose in mice is different due to differences in metabolic rate, pharmacokinetics, and route of administration (van Calsteren et al., 2009). In most rodent studies, DOX is administered i.p. where most of the drug can be taken up by local adipose tissue before entering the systemic circulation. In contrast, cancer patients receive DOX intravenously (i.v.) where it first reaches the endothelial cell layer of the blood vessels and the heart. Detrimental effects on the heart, vasculature, and distant metabolic tissues that occur due to high levels of DOX in the systemic circulation are thus potentially not induced in studies where DOX is injected i.p. such as in this study. However, as several studies reported DOX-induced toxicity in mice after i.p. administration of 2–10 mg/kg DOX, including cardiac toxicity, impaired adipocyte function, and ovarian toxicity (Vergoni et al., 2016; Biondo et al., 2018; Demaria et al., 2017; Pecoraro et al., 2016; dos Silva et al., 2023; Wang et al., 2019), this indicates that the DOX dose that we used is also relevant in mice.

We hypothesized that therapy-induced cellular senescence could play a role in DOX-induced cardiometabolic toxicity as clearance of senescent cells improved DOX-induced liver damage and DOX-induced cardiac dysfunction in mice (Baar et al., 2017; Demaria et al., 2017; Lérida-Viso et al., 2022). However, we did not find an increase in p16^{Ink4a+}-senescent cells or a clear increase in SASP factors after different DOX treatment regimens in multiple tissues of two independent mouse models. Only a few SASP-markers were elevated in gWAT, which could also reflect local inflammation observed in response to DOX administration. In line with our findings, a study by Lérida-Viso et al. (Lérida-Viso et al., 2022) found no difference in *p16*^{Ink4a} and *p21* expression in heart tissue of wild-type C57BL/6 J mice treated with 1 × 10 mg/kg DOX. Treatment of the same mice with 8 × 2.5 mg/kg DOX did result in a significant increase in *p16*^{Ink4a} and *p21*, which was reduced upon treatment with the senolytic drug Navitoclax, however this cumulative DOX dosage was twice as high as in our study. Our findings are in contrast with studies by Demaria et al. (Demaria et al., 2017), who found increased *p16*^{Ink4a} expression in skin, lung, liver, and heart after 1 × 10 mg/kg DOX, and Wang et al. *(*Wang et al., *2022a)*, who used 3 × 5 mg/kg DOX and observed increased *p16*^{Ink4a} expression in kidney. While these studies also used *p16-3MR* mice, they were not on

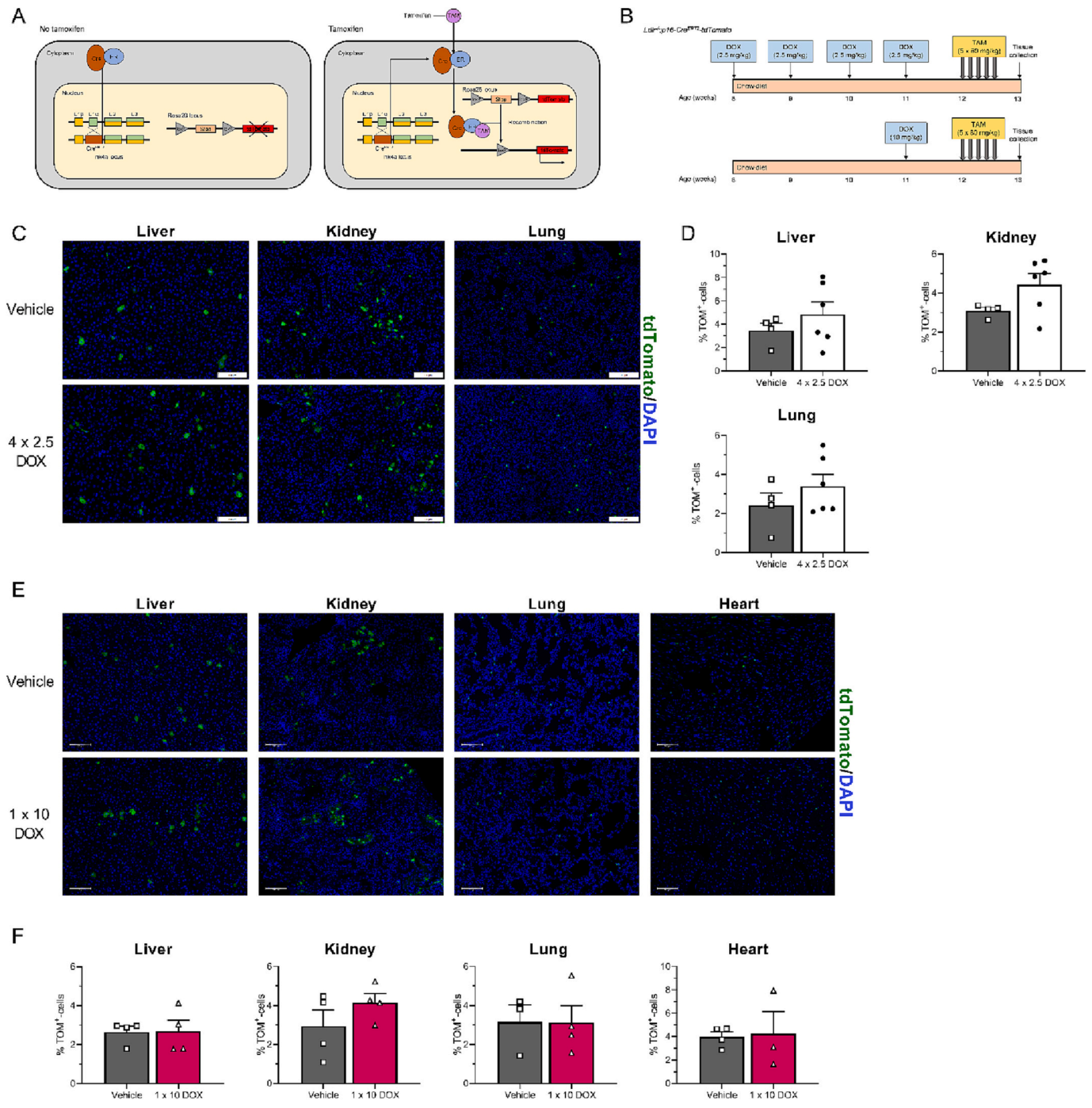

Fig. 8. Different DOX treatment regimens do not induce p16^{Ink4a+}-senescent cell accumulation in *Ldlr*$^{-/-}$*-p16-Cre*^{ERT2}*-tdTomato* mice. (A) Schematic representation of the *p16-Cre*^{ERT2}*-tdTomato* mouse model. (B) Experimental timeline of the different DOX treatment regimens in *Ldlr*$^{-/-}$*-p16-Cre*^{ERT2}*-tdTomato* mice. (C) Representative immunofluorescent staining against tdTomato (green secondary antibody) in liver, kidney, and lung tissue, and (D) the corresponding quantifications presented as % of TOM^{+}-cells of total DAPI^{+}-cells ($n = 4$–6). (E) Representative immunofluorescent images of liver, kidney, lung, and heart stained against tdTomato (green) and (F) the corresponding quantifications ($n = 3$–4). Mice used in (C) and (D) were female, whereas mice used in (E) and (F) were male. Data are presented as mean ± SEM. (For interpretation of the references to colour in this figure legend, the reader is referred to the web version of this article.)

an LDLR-deficient background. In addition, these studies used a mix of males and females for their experiments whereas we used females only. As female mice are reported to be more resistant to DOX-toxicity compared to male mice (Norton et al., 2021; Grant et al., 2019) this could potentially explain the discrepancy in outcome. To test this, we also treated male mice with 1 × 10 mg/kg DOX but also did not observe an increase in *p16*^{Ink4a} expression in liver, kidney, lung, and heart (Fig. 8E, F). Therefore, sex differences in DOX sensitivity do not appear to explain the lack of *p16*^{Ink4a} expression in our study. Furthermore, several studies reported ovarian toxicity in female mice upon 7.5–10 mg/kg DOX administration indicating that female mice are susceptible to DOX-induced toxicity (Pecoraro et al., 2016; dos Silva et al., 2023; Ben-Aharon et al., 2010). As DOX is widely used in women with breast cancer (Christowitz et al., 2019), it is important to elucidate potential sex differences in long-term adverse effects of DOX.

The gonadal adipose tissue depot did show an upregulation of *p21*

both acutely after DOX and after 12 weeks of HFC-diet feeding, which could indicate short-term cell-cycle arrest in response to acute DNA damage or persistent cell-cycle inhibition associated with senescence. A recent study by Wang et al. *(Wang et al., 2022b)* showed that $p21^{+}$-senescent cells and $p16^{Ink4a+}$-senescent cells are two distinct cell populations and that specifically $p21^{+}$-senescent cells in adipose tissue play a causal role in metabolic dysfunction during obesity. Induction of p21-mediated senescence in adipocyte precursors could be a potential explanation for the reduction in gonadal adipose tissue mass after DOX, as senescent preadipocytes lose the ability to proliferate and develop into mature lipid-storing adipocytes (Xu et al., 2015). However, despite the possible loss of adipocyte precursors, we did not observe a detrimental effect on glucose homeostasis after DOX treatment. Clearance of $p16^{Ink4a+}$-senescent cells did not restore gWAT mass in our mice, but since $p21^{+}$-cells were not targeted in our model they could still be a potential player in the detrimental effects of DOX on gWAT. However, as other markers of cellular senescence, such as SASP factors, were not clearly increased, it remains unclear whether these $p21^{+}$- cells represent senescent cells.

Discrepancies in the impact of DOX on metabolic health could also be due to different DOX treatment regimens or the use of different mouse models. First of all, we did not assess long-term metabolic health in our 1×10 mg/kg and 3×5 mg/kg DOX-treated mice. Therefore, we cannot rule out the possibility that these DOX dosing regimens do sensitize mice to develop cardiometabolic disease later in life. Secondly, we used atherosclerosis-prone *Ldlr*$^{-/-}$ mice, in which atherosclerosis is driven by very high plasma cholesterol levels, which were not affected by DOX administration. If DOX treatment mainly results in early initiation of atherosclerosis through the induction of endothelial dysfunction rather than atherosclerosis progression, these effects could be masked by the lipid-overload in *Ldlr*$^{-/-}$ mice. Lastly, the mice used in this study were young-adults, which could be more flexible in resolving DOX-induced damage than older mice. It is thus possible that DOX-induced senescent cells have been cleared more efficiently by the immune system at the time metabolic outcomes were evaluated, as senescent cells are more prone to be cleared by the immune system in young mice than in aged mice (Karin et al., 2019). However, if DOX-induced senescent cells are a major player in cardiometabolic toxicity, we would still have expected a significant senescence induction acutely after DOX in our chow-fed mice.

Clearance of $p16^{Ink4a+}$-senescent cells did not affect atherosclerotic lesion size in our HFC-diet fed *Ldlr*$^{-/-}$*-p16-3MR* mice. These findings are in line with results obtained by Garrido et al. (Garrido et al., 2022), who treated *ApoE*$^{-/-}$*-p16-3MR* mice with GCV and found no detectable differences in plaque size. In contrast, a study by Childs et al. (Childs et al., 2016) showed that removal of $p16^{Ink4a+}$-senescent cells by GCV resulted in a $\sim$ 50% reduction in atherosclerotic plaque size using the same *Ldlr*$^{-/-}$*-p16-3MR* mice and a similar period of HFC-diet feeding. However, we only administered GCV to mice that received DOX and can therefore not rule out that beneficial effects of senescent cell clearance were mitigated by the presence of DOX. In addition, in a follow-up study Childs et al. (Childs et al., 2021) reported that senescent cells induce fibrous cap thinning, which was restored after treatment with the senolytic drug ABT-263. In contrast, in our mouse model and in the study of Garrido et al. (Garrido et al., 2022), necrotic core size and fibrous cap thickness were not affected after $p16^{Ink4a+}$-senescent cell elimination. Together, these results indicate that genetic removal of $p16^{Ink4a+}$-senescent cells does not alleviate the development of atherosclerosis.

In conclusion, our study demonstrates that treatment of young adult female *Ldlr*$^{-/-}$*-p16-3MR* mice with four weekly injections of 2.5 mg/kg DOX does not exacerbate $p16^{Ink4a+}$-senescent cell accumulation or cardiometabolic disease development in response to an HFC-diet. Furthermore, clearance of $p16^{Ink4a+}$-cells does not improve diet-induced metabolic disturbances in our mouse model. Therefore, we conclude that studies reporting a role for DOX-induced $p16^{Ink4a}$-senescent cells in cardiometabolic disease should be interpreted with caution and that the impact of DOX on metabolic health warrants further research to understand the molecular link between cancer therapy and increased risk of cardiometabolic disease in cancer survivors.

Funding

This work was supported by grants from the UMCG Cancer Research Fund (to JWJ), Beatrix Children's Hospital (to JWJ), Dutch Diabetes Research Foundation (Diabetes II Breakthrough project 459001005 to JKK), and Stichting De Cock-Hadders (to ACP). This project was co-financed by the Ministry of Economic Affairs and Climate Policy by means of the PPP-allowance made available by Health~Holland, Top Sector Life Sciences & Health to stimulate public-private partnerships.

CRediT authorship contribution statement

Andrea C. Postmus: Conceptualization, Methodology, Writing – original draft, Formal analysis, Investigation, Visualization, Project administration. **Janine K. Kruit:** Conceptualization, Methodology, Investigation, Writing – review & editing, Supervision, Funding acquisition. **Roos E. Eilers:** Investigation. **Rick Havinga:** Investigation. **Mirjam H. Koster:** Investigation. **Yoshikazu Johmura:** Resources. **Makoto Nakanishi:** Resources. **Bart van de Sluis:** Conceptualization, Methodology, Writing – review & editing, Supervision. **Johan W. Jonker:** Conceptualization, Methodology, Writing – review & editing, Supervision, Funding acquisition, Project administration.

Declaration of Competing Interest

The authors declare no conflicts of interest.

Data availability

Data will be made available on request.

Acknowledgements

The authors would like to thank Manzira Kuerbanjiang, Anouk La Rose, and Tess Yntema for excellent technical assistance, Bertien Dethmers-Ausema for help with performing blood cell counts, and Tim Eijgenraam for help with the echocardiography of the heart.

Appendix A. Supplementary data

Supplementary data to this article can be found online at https://doi.org/10.1016/j.taap.2023.116531.

References

Baar, M.P., Brandt, R.M.C., Putavet, D.A., Klein, J.D.D., Derks, K.W.J., Bourgeois, B.R.M., Stryeck, S., Rijksen, Y., van Willigenburg, H., Feijtel, D.A., van der Pluijm, I., Essers, J., van Cappellen, W.A., van IJcken, W.F., Houtsmuller, A.B., Pothof, J., de Bruin, R.W.F., Madl, T., Hoeijmakers, J.H.J., Campisi, J., de Keizer, P.L.J., 2017. Targeted apoptosis of senescent cells restores tissue homeostasis in response to chemotoxicity and aging. Cell 169 (1), 132. https://doi.org/10.1016/J.CELL.2017.02.031.

Baboota, R.K., Spinelli, R., Erlandsson, M.C., Brandao, B.B., Lino, M., Yang, H., Mardinoglu, A., Bokarewa, M.I., Boucher, J., Kahn, C.R., Smith, U., 2022. Chronic hyperinsulinemia promotes human hepatocyte senescence. Molecular Metabolism 64. https://doi.org/10.1016/J.MOLMET.2022.101558.

Baker, L.H., Boonstra, P.S., Reinke, D.K., Antalis, E.J.P., Zebrack, B.J., Weinberg, R.L., 2020. Burden of chronic diseases among sarcoma survivors treated with anthracycline chemotherapy: results from an observational study. Journal of Cancer Metastasis and Treatment 6. https://doi.org/10.20517/2394-4722.2020.36.

Ben-Aharon, I., Bar-Joseph, H., Tzarfaty, G., Kuchinsky, L., Rizel, S., Stemmer, S.M., Shalgi, R., 2010. Doxorubicin-induced ovarian toxicity. Reprod. Biol. Endocrinol. 8 (1), 1–7. https://doi.org/10.1186/1477-7827-8-20/FIGURES/5.

Ben-Yakov, G., Alao, H., Haydek, J.P., Fryzek, N., Cho, M.H., Hemmati, M., Samala, V., Shovlin, M., Dunleavy, K., Wilson, W., Jones, E.C., Rotman, Y., 2018. Development

of hepatic steatosis after chemotherapy for non-Hodgkin lymphoma. Hepatology Communications 3 (2), 220–226. https://doi.org/10.1002/HEP4.1304.
Biondo, L.A., Batatinha, H.A., Souza, C.O., Teixeira, A.A.S., Silveira, L.S., Alonso-Vale, M. I., Oyama, L.M., Alves, M.J., Seelaender, M., Neto, J.C.R., 2018. Metformin mitigates fibrosis and glucose intolerance induced by doxorubicin in subcutaneous adipose tissue. Front. Pharmacol. 9 (MAY) https://doi.org/10.3389/FPHAR.2018.00452.
Bleyer, A., O'Leary, M., Barr, R., Ries, L.A.G., 2006. Cancer Epidemiology in Older Adolescents and Young Adults 15 to 29 Years of Age, Including SEER Incidence and Survival: 1975-2000. National Cancer Institute, NIH Pub. No. 06-5767, Bethesda, MD.
Bligh, E.G., Dyer, W.J., 1959. A rapid method of total lipid extraction and purification. Can. J. Biochem. Physiol. 37 (8), 911–917. https://doi.org/10.1139/O59-099.
Bonnet, L., Alexandersson, I., Baboota, R.K., Kroon, T., Oscarsson, J., Smith, U., Boucher, J., 2022. Cellular senescence in hepatocytes contributes to metabolic disturbances in NASH. Front. Endocrinol. 13 https://doi.org/10.3389/FENDO.2022.957616.
Childs, B.G., Baker, D.J., Kirkland, J.L., Campisi, J., Deursen, J.M., 2014. Senescence and apoptosis: dueling or complementary cell fates? EMBO Rep. 15 (11), 1139–1153. https://doi.org/10.15252/EMBR.201439245.
Childs, B.G., Baker, D.J., Wijshake, T., Conover, C.A., Campisi, J., van Deursen, J.M., 2016. Senescent intimal foam cells are deleterious at all stages of atherosclerosis. Science (New York, N.Y.) vol. 354 (6311), 472–477. https://doi.org/10.1126/SCIENCE.AAF6659.
Childs, B.G., Zhang, C., Shuja, F., Sturmlechner, I., Trewartha, S., Velasco, R.F., Baker, D. J., Li, H., van Deursen, J.M., 2021. Senescent cells suppress innate smooth muscle cell repair functions in atherosclerosis. Nature Aging 1 (8), 698–714. https://doi.org/10.1038/S43587-021-00089-5.
Christowitz, C., Davis, T., Isaacs, A., van Niekerk, G., Hattingh, S., Engelbrecht, A.M., 2019. Mechanisms of doxorubicin-induced drug resistance and drug resistant tumour growth in a murine breast tumour model. BMC Cancer 19 (1), 1–10. https://doi.org/10.1186/S12885-019-5939-Z/FIGURES/5.
Clayton, Z.S., Hutton, D.A., Mahoney, S.A., Seals, D.R., 2021. Anthracycline chemotherapy-mediated vascular dysfunction as a model of accelerated vascular aging. Aging and Cancer 2 (1–2), 45–69. https://doi.org/10.1002/AAC2.12033.
Daugherty, A., Tall, A.R., Daemen, M.J.A.P., Falk, E., Fisher, E.A., García-Cardeña Lusis, A.J., Owens, P., Rosenfeld, M.E., Virmani, R., 2017. Recommendation on design, execution, and reporting of animal atherosclerosis studies: A scientific statement from the American Heart Association. Arterioscler. Thromb. Vasc. Biol. 37 (9), e131–e157. https://doi.org/10.1161/ATV.0000000000000062.
de Haas, E.C., Oosting, S.F., Lefrandt, J.D., Wolffenbuttel, B.H., Sleijfer, D.T., Gietema, J. A., 2010. The metabolic syndrome in cancer survivors. The Lancet. Oncology 11 (2), 193–203. https://doi.org/10.1016/S1470-2045(09)70287-6.
de Lima Junior, E.A., Yamashita, A.S., Pimentel, G.D., de Sousa, L.G.O., Santos, R.V.T., Gonçalves, C.L., Streck, E.L., de Lira, F.S., Rosa Neto, J.C., 2016. Doxorubicin caused severe hyperglycaemia and insulin resistance, mediated by inhibition in AMPk signalling in skeletal muscle. J. Cachexia. Sarcopenia Muscle 7 (5), 615–625. https://doi.org/10.1002/JCSM.12104.
Demaria, M., Ohtani, N., Youssef, S.A., Rodier, F., Toussaint, W., Mitchell, J.R., Laberge, R.M., Vijg, J., VanSteeg, H., Dollé, M.E.T., Hoeijmakers, J.H.J., deBruin, A., Hara, E., Campisi, J., 2014. An essential role for senescent cells in optimal wound healing through secretion of PDGF-AA. Dev. Cell 31 (6), 722–733. https://doi.org/10.1016/J.DEVCEL.2014.11.012.
Demaria, M., O'Leary, M.N., Chang, J., Shao, L., Liu, S., Alimirah, F., Koenig, K., Le, C., Mitin, N., Deal, A.M., Alston, S., Academia, E.C., Kilmarx, S., Valdovinos, A., Wang, B., de Bruin, A., Kennedy, B.K., Melov, S., Zhou, D., et al., 2017. Cellular senescence promotes adverse effects of chemotherapy and cancer relapse. Cancer Discovery 7 (2), 165–176. https://doi.org/10.1158/2159-8290.CD-16-0241.
Dieli-Conwright, C.M., Wong, L., Waliany, S., Mortimer, J.E., 2022. Metabolic syndrome and breast cancer survivors: a follow-up analysis after completion of chemotherapy. Diabetology & Metabolic Syndrome 14 (1). https://doi.org/10.1186/S13098-022-00807-Y.
dos Silva, R.L., Lins, T.L.B.G., Monte, A.P.O., Andrade, K.O., Sousa Barberino, R., Silva, G.A.L., Campinho, D.S.P., Junior, R.C.P., Matos, M.H.T., 2023. Protective effect of gallic acid on doxorubicin-induced ovarian toxicity in mouse. Reproductive Toxicology (Elmsford, N.Y.) 115, 147–156. https://doi.org/10.1016/J.REPROTOX.2022.12.008.
Dowling, E.C., Chawla, N., Forsythe, L.P., de Moor, J., McNeel, T., Rozjabek, H.M., Ekwueme, D.U., Yabroff, K.R., 2013. Lost productivity and burden of illness in cancer survivors with and without other chronic conditions. Cancer 119 (18), 3393–3401. https://doi.org/10.1002/CNCR.28214.
Freund, A., Laberge, R.M., Demaria, M., Campisi, J., 2012. Lamin B1 loss is a senescence-associated biomarker. Mol. Biol. Cell 23 (11), 2066–2075. https://doi.org/10.1091/MBC.E11-10-0884.
Garrido, A.M., Kaistha, A., Uryga, A.K., Oc, S., Foote, K., Shah, A., Finigan, A., Figg, N., Dobnikar, L., Jørgensen, H., Bennett, M., 2022. Efficacy and limitations of senolysis in atherosclerosis. Cardiovasc. Res. 118 (7), 1713–1727. https://doi.org/10.1093/CVR/CVAB208.
Grant, M.K.O., Seelig, D.M., Sharkey, L.C., Choi, W.S.V., Abdelgawad, I.Y., Zordoky, B. N., 2019. Sexual dimorphism of acute doxorubicin-induced nephrotoxicity in C57Bl/6 mice. PLoS One 14 (2), e0212486. https://doi.org/10.1371/JOURNAL.PONE.0212486.
He, S., Sharpless, N.E., 2017. Senescence in health and disease. Cell 169 (6), 1000–1011. https://doi.org/10.1016/J.CELL.2017.05.015.
Hutton, D., Brunt, V., Mahoney, S., Casso, A., Greenberg, N., VanDongen, N., Ziemba, B., Nguyen, K., Melov, S., Campisi, J., Seals, D., Clayton, Z., 2021. Cellular senescence mediates doxorubicin-induced arterial dysfunction via activation of mitochondrial oxidative stress and the mammalian target of rapamycin. FASEB J. 35 (S1) https://doi.org/10.1096/FASEBJ.2021.35.S1.00283.
Juanjuan, L., Wen, W., Zhongfen, L., Chuang, C., Jing, C., Yiping, G., Changhua, W., Dehua, Y., Shengrong, S., 2015. Clinical pathological characteristics of breast cancer patients with secondary diabetes after systemic therapy: a retrospective multicenter study. Tumour Biology 36 (9), 6939–6947. https://doi.org/10.1007/S13277-015-3380-8.
Karimian, A., Ahmadi, Y., Yousefi, B., 2016. Multiple functions of p21 in cell cycle, apoptosis and transcriptional regulation after DNA damage. DNA Repair 42, 63–71. https://doi.org/10.1016/J.DNAREP.2016.04.008.
Karin, O., Agrawal, A., Porat, Z., Krizhanovsky, V., Alon, U., 2019. Senescent cell turnover slows with age providing an explanation for the Gompertz law. Nature Communications 10 (1). https://doi.org/10.1038/S41467-019-13192-4.
Keegan, T.H.M., Ries, L.A.G., Barr, R.D., Geiger, A.M., Dahlke, D.V., Pollock, B.H., Bleyer, W.A., 2016. Comparison of cancer survival trends in the United States of adolescents and young adults with those in children and older adults. Cancer 122 (7), 1009–1016. https://doi.org/10.1002/CNCR.29869.
Lahoti, S., Patel, D., Thekkemadom, V., Beckett, R., Ray, D., 2012. Doxorubicin-induced in vivo nephrotoxicity involves oxidative stress-mediated multiple pro- and anti-apoptotic signaling pathways. Curr. Neurovasc. Res. 9 (4), 282–295. https://doi.org/10.2174/156720212803530636.
Lérida-Viso, A., Estepa-Fernández, A., Morellá-Aucejo, Á., Lozano-Torres, B., Alfonso, M., Blandez, J.F., Bisbal, V., Sepúlveda, P., García-Fernández, A., Orzáez, M., Martínez-Máñez, R., 2022. Pharmacological senolysis reduces doxorubicin-induced cardiotoxicity and improves cardiac function in mice. Pharmacol. Res. 183 https://doi.org/10.1016/J.PHRS.2022.106356.
Liu, L., Moke, D.J., Tsai, K.Y., Hwang, A., Freyer, D.R., Hamilton, A.S., Zhang, J., Cockburn, M., Deapen, D., 2019. A reappraisal of sex-specific cancer survival trends among adolescents and young adults in the United States. J. Natl. Cancer Inst. 111 (5), 509–518. https://doi.org/10.1093/JNCI/DJY140.
Luo, L., Liu, M., 2016. Adipose tissue in control of metabolism. J. Endocrinol. 231 (3), R77–R99. https://doi.org/10.1530/JOE-16-0211.
Luu, A.Z., Chowdhury, B., Al-Omran, M., Teoh, H., Hess, D.A., Verma, S., 2018. Role of endothelium in doxorubicin-induced cardiomyopathy. JACC. Basic to Translational Science 3 (6), 861–870. https://doi.org/10.1016/J.JACBTS.2018.06.005.
Mitry, M.A., Edwards, J.G., 2016. Doxorubicin induced heart failure: phenotype and molecular mechanisms. IJC Heart Vasc. 10, 17–24. https://doi.org/10.1016/J.IJCHA.2015.11.004.
Mohan, U.P., Tirupathi Pichiah, P.B., Iqbal, S.T.A., Arunachalam, S., 2021. Mechanisms of doxorubicin-mediated reproductive toxicity - A review. Reproductive Toxicology (Elmsford, N.Y.) 102, 80–89. https://doi.org/10.1016/J.REPROTOX.2021.04.003.
Moore, K.J., Sheedy, F.J., Fisher, E.A., 2013. Macrophages in atherosclerosis: a dynamic balance. Nat. Rev. Immunol. 13 (10), 709–721. https://doi.org/10.1038/NRI3520.
Norton, N., Bruno, K.A., Florio, D.N., Whelan, E.R., Hill, A.R., Morales-Lara, A.C., Mease, A.A., Sousou, J.M., Malavet, J.A., Dorn, L.E., Salomon, G.R., Macomb, L.P., Khatib, S., Anastasiadis, Z.P., Necela, B.M., McGuire, M.M., Giresi, P.G., Kotha, A., Beetler, D.J., et al., 2021. Trpc6 promotes doxorubicin-induced cardiomyopathy in male mice with pleiotropic differences between males and females. Frontiers in Cardiovascular Medicine 8, 757784. https://doi.org/10.3389/FCVM.2021.757784.
Omori, S., Wang, T.W., Johmura, Y., Kanai, T., Nakano, Y., Kido, T., Susaki, E.A., Nakajima, T., Shichino, S., Ueha, S., Ozawa, M., Yokote, K., Kumamoto, S., Nishiyama, A., Sakamoto, T., Yamaguchi, K., Hatakeyama, S., Shimizu, E., Katayama, K., et al., 2020. Generation of a p16 reporter mouse and its use to characterize and target p16high cells in vivo. Cell Metab. 32 (5), 814–828.e6. https://doi.org/10.1016/J.CMET.2020.09.006.
Pecoraro, M., Del Pizzo, M., Marzocco, S., Sorrentino, R., Ciccarelli, M., Iaccarino, G., Pinto, A., Popolo, A., 2016. Inflammatory mediators in a short-time mouse model of doxorubicin-induced cardiotoxicity. Toxicol. Appl. Pharmacol. 293, 44–52.
Postmus, A.C., Sturmlechner, I., Jonker, J.W., van Deursen, J.M., van de Sluis, B., Kruit, J.K., 2019. Senescent cells in the development of cardiometabolic disease. Curr. Opin. Lipidol. 30 (3), 177–185. https://doi.org/10.1097/MOL.0000000000000602.
Prasanna, P.L., Renu, K., Valsala Gopalakrishnan, A., 2020. New molecular and biochemical insights of doxorubicin-induced hepatotoxicity. Life Sci. 250 https://doi.org/10.1016/J.LFS.2020.117599.
Quagliariello, V., de Laurentiis, M., Rea, D., Barbieri, A., Monti, M.G., Carbone, A., Paccone, A., Altucci, L., Conte, M., Canale, M.L., Botti, G., Maurea, N., 2021. The SGLT-2 inhibitor empagliflozin improves myocardial strain, reduces cardiac fibrosis and pro-inflammatory cytokines in non-diabetic mice treated with doxorubicin. Cardiovasc. Diabetol. 20 (1) https://doi.org/10.1186/S12933-021-01346-Y.
Rahimi, O., Melo, A.C., Westwood, B., Grier, R.D.M., Tallant, E.A., Gallagher, P.E., 2022. Angiotensin-(1-7) reduces doxorubicin-induced aortic arch dysfunction in male and female juvenile Sprague Dawley rats through pleiotropic mechanisms. Peptides 152. https://doi.org/10.1016/J.PEPTIDES.2022.170784.
Reagan-Shaw, S., Nihal, M., Ahmad, N., 2008. Dose translation from animal to human studies revisited. FASEB Journal 22 (3), 659–661. https://doi.org/10.1096/FJ.07-9574LSF.
Renu, K., Sruthy, K.B., Parthiban, S., Sugunapriyadharshini, S., George, A., Tirupathi, T. P., Suman, S., Abilash, V.G., Arunachalam, S., 2019. Elevated lipolysis in adipose tissue by doxorubicin via PPARα activation associated with hepatic steatosis and insulin resistance. Eur. J. Pharmacol. 843, 162–176. https://doi.org/10.1016/J.EJPHAR.2018.11.018.
Sauter, K.A.D., Wood, L.J., Wong, J., Iordanov, M., Magun, B.E., 2011. Doxorubicin and daunorubicin induce processing and release of interleukin-1β through activation of the NLRP3 inflammasome. Cancer Biology & Therapy 11 (12), 1008–1016. https://doi.org/10.4161/CBT.11.12.15540.

Sedeman, M., Christowitz, C., de Jager, L., Engelbrecht, A.M., 2022. Obese mammary tumour-bearing mice are highly sensitive to doxorubicin-induced hepatotoxicity. BMC Cancer 22 (1). https://doi.org/10.1186/S12885-022-10189-Z.

Seimon, T.A., Wang, Y., Han, S., Senokuchi, T., Schrijvers, D.M., Kuriakose, G., Tall, A.R., Tabas, I.A., 2009. Macrophage deficiency of p38alpha MAPK promotes apoptosis and plaque necrosis in advanced atherosclerotic lesions in mice. J. Clin. Invest. 119 (4), 886–898. https://doi.org/10.1172/JCI37262.

Sharma, M., Tuaine, J., McLaren, B., Waters, D.L., Black, K., Jones, L.M., McCormick, S.P. A., 2016. Chemotherapy agents alter plasma lipids in breast cancer patients and show differential effects on lipid metabolism genes in liver cells. PLoS One 11 (1). https://doi.org/10.1371/JOURNAL.PONE.0148049.

Shimizu, N., Ngayama, D., Watanabe, Y., Yamaguchi, T., Nakamura, S., Ohira, M., Saiki, A., Onda, H., Yamaoka, S., Abe, K., Nakaseko, C., Tatsuno, I., 2022. Rituximab, cyclophosphamide, doxorubicin, vincristine, and prednisolone (R-CHOP) therapy increases carotid intima-media thickness and plaque score with von Willebrand factor activity elevation in patients with malignant lymphoma. Journal of Chemotherapy (Florence, Italy) 34 (4), 258–263. https://doi.org/10.1080/1120009X.2021.1988202.

Smitherman, A.B., Wood, W.A., Mitin, N., Ayer Miller, V.L., Deal, A.M., Davis, I.J., Blatt, J., Gold, S.H., Muss, H.B., 2020. Accelerated aging among childhood, adolescent, and young adult cancer survivors is evidenced by increased expression of p16INK4a and frailty. Cancer 126 (22), 4975–4983. https://doi.org/10.1002/CNCR.33112.

Song, W., Wang, H., Wu, Q., 2015. Atrial natriuretic peptide in cardiovascular biology and disease (NPPA). Gene 569 (1), 1. https://doi.org/10.1016/J.GENE.2015.06.029.

Stelwagen, J., Lubberts, S., Steggink, L.C., Steursma, G., Kruyt, L.M., Donkerbroek, J.W., van Roon, A.M., van Gessel, A.I., van de Zande, S.C., Meijer, C., Gräfin Zu Eulenburg, C.H., Oosting, S.F., Nuver, J., Walenkamp, A.M.E., Jan de Jong, I., Lefrandt, J.D., Gietema, J.A., 2020. Vascular aging in long-term survivors of testicular cancer more than 20 years after treatment with cisplatin-based chemotherapy. Br. J. Cancer 123 (11), 1599–1607. https://doi.org/10.1038/S41416-020-01049-3.

Thorn, C.F., Oshiro, C., Marsh, S., Hernandez-Boussard, T., McLeod, H., Klein, T.E., Altman, R.B., 2011. Doxorubicin pathways: pharmacodynamics and adverse effects. Pharmacogenet. Genomics 21 (7), 440–446. https://doi.org/10.1097/FPC.0B013E32833FFB56.

van Calsteren, K., Hartmann, D., van Aerschot, L., Verbesselt, R., van Bree, R., D'Hooge, R., Amant, F., 2009. Vinblastine and doxorubicin administration to pregnant mice affects brain development and behaviour in the offspring. Neurotoxicology 30 (4), 647–657. https://doi.org/10.1016/J.NEURO.2009.04.009.

van Deursen, J.M., 2014. The role of senescent cells in ageing. Nature 509 (7501), 439–446. https://doi.org/10.1038/nature13193.

Vergoni, B., Cornejo, P.J., Gilleron, J., Djedaini, M., Ceppo, F., Jacquel, A., Bouget, G., Ginet, C., Gonzalez, T., Maillet, J., Dhennin, V., Verbanck, M., Auberger, P., Froguel, P., Tanti, J.F., Cormont, M., 2016. DNA damage and the activation of the p53 pathway mediate alterations in metabolic and secretory functions of adipocytes. Diabetes 65 (10), 3062–3074. https://doi.org/10.2337/DB16-0014.

Volkova, M., Russell, R., 2011. Anthracycline cardiotoxicity: prevalence, pathogenesis and treatment. Curr. Cardiol. Rev. 7 (4), 214–220. https://doi.org/10.2174/157340311799960645.

Wang, Y., Liu, M., Johnson, S.B., Yuan, G., Arriba, A.K., Zubizarreta, M.E., Chatterjee, S., Nagarkatti, M., Nagarkatti, P., Xiao, S., 2019. Doxorubicin obliterates mouse ovarian reserve through both primordial follicle atresia and overactivation. Toxicol. Appl. Pharmacol. 381 https://doi.org/10.1016/J.TAAP.2019.114714.

Wang, B., Wang, L., Gasek, N.S., Zhou, Y., Kim, T., Guo, C., Jellison, E.R., Haynes, L., Yadav, S., Tchkonia, T., Kuchel, G.A., Kirkland, J.L., Xu, M., 2021. An inducible p21-Cre mouse model to monitor and manipulate p21-highly-expressing senescent cells in vivo. Nature Aging 1 (10), 962–973. https://doi.org/10.1038/S43587-021-00107-6.

Wang, B., Varela-Eirin, M., Brandenburg, S.M., Hernandez-Segura, A., van Vliet, T., Jongbloed, E.M., Wilting, S.M., Ohtani, N., Jager, A., Demaria, M., 2022a. Pharmacological CDK4/6 inhibition reveals a p53-dependent senescent state with restricted toxicity. EMBO J. 41 (6) https://doi.org/10.15252/EMBJ.2021108946.

Wang, L., Wang, B., Gasek, N.S., Zhou, Y., Cohn, R.L., Martin, D.E., Zuo, W., Flynn, W.F., Guo, C., Jellison, E.R., Kim, T., Prata, L.G.P.L., Palmer, A.K., Li, M., Inman, C.L., Barber, L.S., Al-Naggar, I.M.A., Zhou, Y., Du, W., et al., 2022b. Targeting p21Cip1 highly expressing cells in adipose tissue alleviates insulin resistance in obesity. Cell Metab. 34 (1), 75–89.e8. https://doi.org/10.1016/J.CMET.2021.11.002.

Wiley, C.D., Liu, S., Limbad, C., Zawadzka, A.M., Beck, J., Demaria, M., Artwood, R., Alimirah, F., Lopez-Dominguez, J.A., Kuehnemann, C., Danielson, S.R., Basisty, N., Kasler, H.G., Oron, T.R., Desprez, P.Y., Mooney, S.D., Gibson, B.W., Schilling, B., Campisi, J., Kapahi, P., 2019. SILAC analysis reveals increased secretion of hemostasis-related factors by senescent cells. Cell Rep. 28 (13), 3329–3337.e5. https://doi.org/10.1016/j.celrep.2019.08.049.

Xu, M., Palmer, A.K., Ding, H., Weivoda, M.M., Pirtskhalava, T., White, T.A., Sepe, A., Johnson, K.O., Stout, M.B., Giorgadze, N., Jensen, M.D., LeBrasseur, N.K., Tchkonia, T., Kirkland, J.L., 2015. Targeting senescent cells enhances adipogenesis and metabolic function in old age. eLife 4, e12997. https://doi.org/10.7554/eLife.12997.

Xu, M., Pirtskhalava, T., Farr, J.N., Weigand, B.M., Palmer, A.K., Weivoda, M.M., Inman, C.L., Ogrodnik, M.B., Hachfeld, C.M., Fraser, D.G., Onken, J.L., Johnson, K. O., Verzosa, G.C., Langhi, L.G.P., Weigl, M., Giorgadze, N., LeBrasseur, N.K., Miller, J.D., Jurk, D., et al., 2018. Senolytics improve physical function and increase lifespan in old age. Nat. Med. 24 (8), 1246. https://doi.org/10.1038/S41591-018-0092-9.

Young, R.C., Ozols, R.F., Myers, C.E., 1981. The anthracycline antineoplastic drugs. N. Engl. J. Med. 305 (3), 139–153. https://doi.org/10.1056/NEJM198107163050305.